Article

Current Biology

A Forward Genetic Screen in Zebrafish Identifies the G-Protein-Coupled Receptor CaSR as a Modulator of Sensorimotor Decision Making

Graphical Abstract

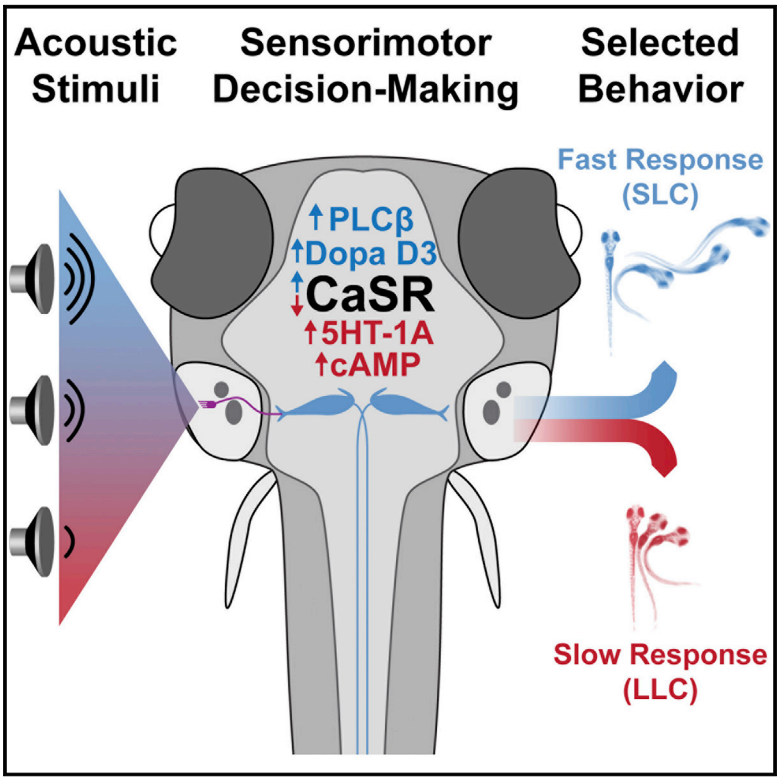

Highlights

- Zebrafish larvae exhibit robust acoustically evoked decision making
- Forward genetic screen identifies sensorimotor decision-making mutants
- Screen reveals a previously unknown role for the G-protein-coupled receptor *CaSR*
- *CaSR* acutely regulates sensorimotor decision making through $G\alpha_{i/o}$ and $G\alpha_{q}$ signaling

Authors

Roshan A. Jain, Marc A. Wolman, Kurt C. Marsden, ..., Amy D. Zamora, Alberto E. Pereda, Michael Granato

Correspondence

rjain1@haverford.edu (R.A.J.), granatom@pennmedicine.upenn.edu (M.G.)

In Brief

Using larval zebrafish, Jain et al. establish and validate a simple sensorimotor decision-making paradigm. Using this paradigm, they perform a forward genetic screen that identifies the first set of vertebrate sensorimotor decision-making genes, including the *calcium-sensing receptor*, which acts as a bidirectional regulator of sensorimotor choice.

Jain et al., 2018, Current Biology *28*, 1357–1369
May 7, 2018
https://doi.org/10.1016/j.cub.2018.03.025

CellPress

Current Biology
Article

A Forward Genetic Screen in Zebrafish Identifies the G-Protein-Coupled Receptor CaSR as a Modulator of Sensorimotor Decision Making

Roshan A. Jain,[1,2,*] Marc A. Wolman,[1,4] Kurt C. Marsden,[1,5] Jessica C. Nelson,[1] Hannah Shoenhard,[1] Fabio A. Echeverry,[3] Christina Szi,[2] Hannah Bell,[1,6] Julianne Skinner,[1] Emilia N. Cobbs,[2] Keisuke Sawada,[2] Amy D. Zamora,[2] Alberto E. Pereda,[3] and Michael Granato[1,7,*]

[1]Department of Cell and Developmental Biology, Perelman School of Medicine, University of Pennsylvania, Philadelphia, PA 19104, USA
[2]Department of Biology, Haverford College, Haverford, PA 19041, USA
[3]Dominick P. Purpura Department of Neuroscience, Albert Einstein College of Medicine, Rose F. Kennedy Center, 1410 Pelham Parkway South, Bronx, NY 10461, USA
[4]Present address: Department of Integrative Biology, University of Wisconsin, Madison, WI 53706, USA
[5]Present address: Department of Biological Sciences, North Carolina State University, Raleigh, NC 27607, USA
[6]Present address: University of Rochester Medical Center, University of Rochester, Rochester, NY 14642, USA
[7]Lead Contact
*Correspondence: rjain1@haverford.edu (R.A.J.), granatom@pennmedicine.upenn.edu (M.G.)
https://doi.org/10.1016/j.cub.2018.03.025

SUMMARY

Animals continuously integrate sensory information and select contextually appropriate responses. Here, we show that zebrafish larvae select a behavioral response to acoustic stimuli from a pre-existing choice repertoire in a context-dependent manner. We demonstrate that this sensorimotor choice is modulated by stimulus quality and history, as well as by neuromodulatory systems—all hallmarks of more complex decision making. Moreover, from a genetic screen coupled with whole-genome sequencing, we identified eight mutants with deficits in this sensorimotor choice, including mutants of the vertebrate-specific G-protein-coupled extracellular calcium-sensing receptor (*CaSR*), whose function in the nervous system is not well understood. We demonstrate that *CaSR* promotes sensorimotor decision making acutely through $G\alpha_{i/o}$ and $G\alpha_{q/11}$ signaling, modulated by clathrin-mediated endocytosis. Combined, our results identify the first set of genes critical for behavioral choice modulation in a vertebrate and reveal an unexpected critical role for *CaSR* in sensorimotor decision making.

INTRODUCTION

Animals navigating their environment are challenged to prioritize one behavior over another. For example, terrestrial and aquatic vertebrates exposed to an abrupt acoustic stimulus can reorient to explore the stimulus source or perform a protective startle response to shield their body or escape a potential predator [1, 2]. The decision to perform one behavior over another depends not only on qualities relating to the stimulus but also on prior experiences and context [2, 3]. Sources of context include the external environment, such as the presence of predators or food, and internal states such as hunger, anxiety, or ongoing behaviors [4]. Across the wide range of decision-making complexity, each decision-making scenario ultimately represents behavioral selection and bias [5].

While decision making can involve complex cognitive computation, simple behavioral choices in invertebrates and non-mammalian vertebrates are also dynamically modulated, providing the opportunity to use genetically tractable systems to study distinct steps of the decision-making process [6–10]. For example, *C. elegans* movement directionality is controlled by forward and backward motor circuits, and the interface between these circuits has been used to study decision making for directional locomotion [11]. Similarly, optogenetic dissection of the mechanosensory responses of *Drosophila* larvae has revealed different inhibitory circuit modules controlling behavioral selection, switching, and maintenance in this simple context [12]. Finally, zebrafish larvae use visually guided decision making to move toward or away from looming stimuli based on size, allowing pursuit of small prey and avoidance of large potential predators [13]. However, the molecular-genetic mechanisms underlying vertebrate decision making, even for simple behavioral choices in larval zebrafish, are not well understood.

To establish a robust decision-making paradigm amenable to genetic screens, we used an evolutionarily conserved and ethologically relevant behavior, the acoustic startle response [14]. In response to acoustic stimuli, zebrafish larvae execute one of two distinct motor behaviors: a short-latency C-bend (SLC) response, initiating within 5–15 ms of the stimulus, or a slower, long-latency C-bend (LLC) response, initiating within 20–80 ms (Figure 1A; Video S1) [15]. Time projection analysis previously revealed that, unlike the SLC response, LLC behavior usually does not displace the animal from its original location during a 40-ms time window typical of fast aquatic predator strikes, suggesting that selecting LLC maneuvers

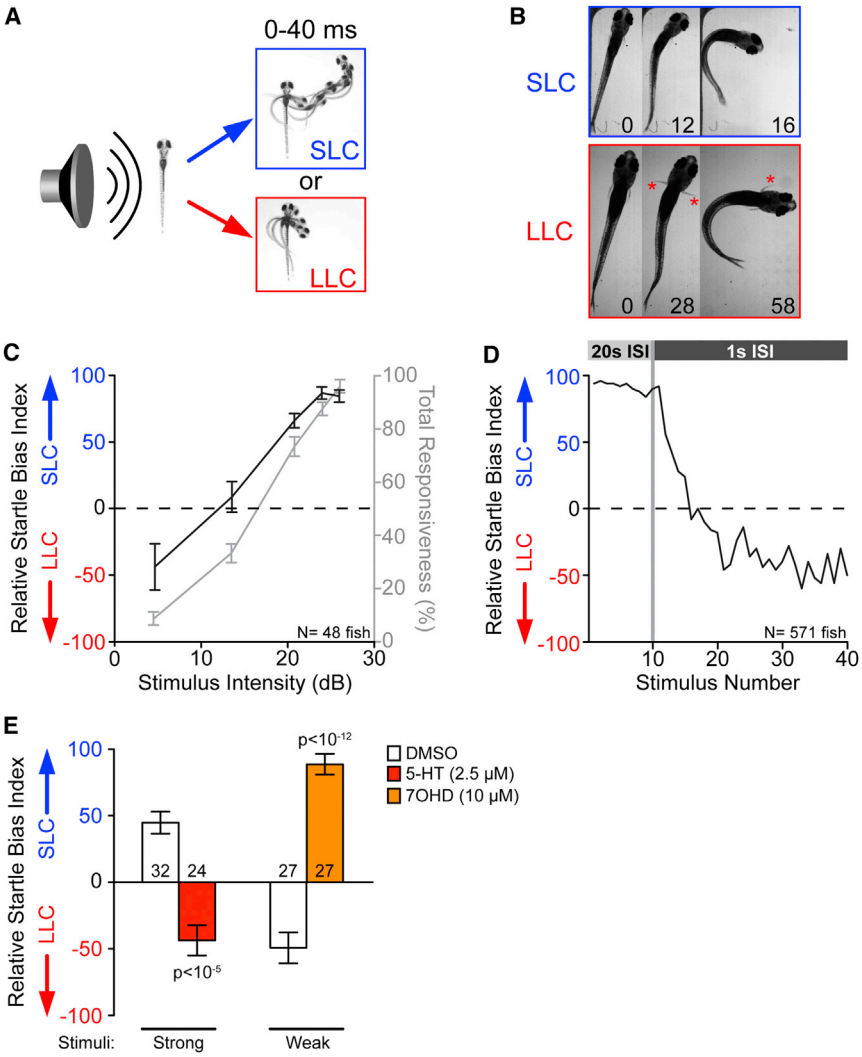

Figure 1. Selection of Appropriate Behavioral Responses to Acoustic Stimuli Is a Dynamic Process

(A) Temporal projections over 40 ms post-stimulus of wild-type 5-dpf larvae performing SLC and LLC behaviors.

(B) Time course of the initial C-bend of wild-type (WIK) fish performing SLC and LLC responses, 16 dpf. Numbers show elapsed time (in milliseconds) after stimulus; red asterisks indicate active pectoral fin usage.

(C) Average behavioral bias (black, left axis) and response frequency (gray, right axis) of 48 larvae (5 dpf) to acoustic stimuli ($p < 0.0001$, Kruskal-Wallis test). Relative startle bias index was calculated for each larva at each intensity (see STAR Methods).

(D) Average relative startle bias of 5-dpf larvae following identical 26-dB stimuli at 20-s intervals (stimuli 1–10) and then 1-s intervals (stimuli 11–40).

(E) Average relative startle bias of 5-dpf larvae treated for 20 min with serotonin (5-HT) or dopamine D3 receptor agonist R-(+)-7-Hydroxy-DPAT (7OHD). Numbers of larvae tested are given at base of bars.

Error bars indicate SEM. See also Figures S1 and S2, Table S1, and Video S1.

would be less effective for evading high-speed attacks (Figure 1A). SLC and LLC responses are also readily distinguishable based on other kinematic parameters, including angular velocity and turning angle [15]. One hallmark of decision making is that distinct neural circuits mediate the different behavioral outcomes. Both SLC and LLC behaviors can be elicited by acoustic/vibrational stimuli, which zebrafish larvae detect through the sensory hair cells of the lateral line (transmitted through the anterior and posterior lateral line ganglia) and the otic vesicle (transmitted via the VIIIth statoacoustic nerve), all of which project to the hindbrain, where they synapse on the lateral dendrite of the Mauthner cell and on other hindbrain neurons [16–18]. Mauthner ablation abolishes SLC responses without affecting LLC behavior, while loss of otoliths in the ear abolishes LLC but not SLC responses [15, 19]. Moreover, ablation of hindbrain spiral fiber neurons decreases SLC responses in favor of LLC responses [19]. Finally, pectoral fins remain adducted during SLC behaviors, while they are active during LLC behaviors (Figure 1B; Video S2) [20]. Thus, while the circuits underlying LLC versus SLC choice have not been fully mapped, SLC and LLC behaviors are not tunable variations of the same motor pattern but utilize different, possibly overlapping, circuitry to generate distinct behaviors.

Here, we establish and validate a robust and high-throughput behavioral paradigm, using larval zebrafish to measure and quantify acoustically driven SLC versus LLC sensorimotor decision making. Using this paradigm, we performed a forward genetic screen and identified the first set of sensorimotor decision-making mutants in a vertebrate, including mutants of the extracellular *calcium-sensing receptor* (*CaSR*). Finally, we demonstrate a previously unknown regulatory role for the extracellular *CaSR* in acutely modulating behavior and identify key downstream effectors and regulators of CaSR signaling modulating sensorimotor decision making *in vivo*.

RESULTS

SLC versus LLC Bias Fulfills Key Criteria Defining Decision Making

To determine whether SLC versus LLC behavioral selection indeed reflects a simple decision behavior, we characterized additional criteria common to many well-established decision-making paradigms [7, 21]. First, we examined whether SLC versus LLC selection simply reflects a fixed bias or whether it is influenced by stimulus quality. We thus examined response bias to a range of acoustic stimulus intensities, where overall responsiveness increased as stimulus intensity increased, consistent with previous observations (Figure 1C) [15]. At weak stimulus intensities (4.6 dB), larvae were strongly biased to select LLC responses, which shifted to relatively unbiased selection at

moderate intensities (13.5 dB) and strong SLC selection bias at high intensities (25.9 dB; Figure 1C). Thus, with increasing stimulus intensity, larvae robustly shift their response bias from LLC to SLC behaviors.

We next tested whether larvae dynamically shift their acoustic response behavior based on prior experience [22]. For this, we exposed larvae to a series of intense stimuli (25.9 dB) at 20-s intervals, followed by a series of 30 equally intense stimuli now spaced 1 s apart (Figure 1D). Although overall stimulus responsiveness eventually declined due to habituation [23], responding larvae rapidly shifted their relative bias from SLC to LLC responses during stimuli 11–20, when responsiveness was still >50% (Figure 1D). Importantly, this dynamic bias shift was not unique to larvae at 5 days postfertilization (dpf), as 29-dpf fish that were exposed to a similar paradigm of repeating stimuli also shifted their bias away from SLC and toward LLC responses (Figure S1), demonstrating that dynamic regulation of acoustic behavior selection in the mature nervous system is already functional in 5-dpf larvae.

Lastly, we tested whether neuromodulation characteristic of more complex decision making also modulates SLC versus LLC choice. We screened a library of 1,280 bioactive molecules with known targets for their acute effects on SLC versus LLC bias. From this screen, we identified 95 compounds shifting bias from SLC to LLC following strong stimuli, and 54 compounds shifting bias from LLC to SLC following weak stimuli. We focused on a molecular subset predicted to modulate neurotransmission, including glutamatergic, cholinergic, purinergic, and GABAergic as well as serotonergic and dopaminergic neurotransmission, observing a significant over-representation of compounds modulating serotonergic neurotransmission among those shifting bias toward LLC responses (Figure S2; Table S1). We confirmed that acute exposure to 5-HT1A receptor agonists (PAPP, S15535, and serotonin) effectively shifted bias from SLC to LLC following intense stimuli (Figures 1E and S2). Conversely, dopaminergic modulators were the largest class of drugs shifting bias toward SLC behavior, and acute exposure to a D3 agonist (7OHD) shifted bias from LLC to SLC following weak stimuli (Figure 1E), while exposure to a D3 antagonist shifted bias toward LLC behavior (Figure S2). Thus, acute pharmacological modulation of serotonergic and dopaminergic neurotransmission significantly and bidirectionally shift the SLC versus LLC sensorimotor choice.

A Forward Genetic Screen Identifies Zebrafish Mutants with Deficits in SLC versus LLC Choice

To identify genes required for simple acoustic decision making, we performed a forward genetic screen in parallel to a previously reported screen for habituation mutants [24], screening third-generation 5-dpf offspring from ENU-mutagenized males for their acoustic response bias. Larvae displaying any morphological phenotypes, hearing defects and/or a low (<40%) overall response rate to strong acoustic stimuli, or strong kinematic defects in the performance of SLC or LLC behaviors, were excluded from further analyses. Through this screen, we identified eight mutants in which response bias to an intense stimulus was significantly shifted from SLC toward LLC responses. We quantified the extent to which SLC versus LLC bias was changed in each mutant (Figure 2A), revealing variations in the strength and/or penetrance of the bias shift phenotype between mutants, from the nearly exclusive LLC-biased responses of *better late than never*^{p193} and *late responder*^{p196} to the milder effect of *procrastinator*^{p192} (Figure 2A). Though most phenotypes were observed at frequencies suggesting recessive effects, the *biased*^{dp197} allele produced a clear bias phenotype in half of the offspring of carrier outcrosses to wild-type, indicating a dominant or haploinsufficient allele. All tested crosses between recessive carriers of different alleles showed phenotypic complementation, indicating that most or all of these mutations represent different genes (Table 1).

To test the behavioral specificity of our mutants, we measured overall acoustic responsiveness, spontaneous swimming activity, and habituation learning, as well as visually evoked turning behaviors (O-bends [25]). All mutants showed mild-to-no reductions in overall responsiveness to 26-dB stimuli, with *fashionably late*^{p191} and *wrong turn*^{p190} showing the largest and smallest reductions, respectively (Table 1). While such changes are not sufficient to account for the large response bias change, as many mutant individuals responded to 100% of stimuli with strong LLC biases, we cannot rule out additional mild impacts on acoustic sensitivity in some mutants. Spontaneous movement levels were indistinguishable from wild-type for *wrong turn*^{p190}, *procrastinator*^{p192}, *better late than never*^{p193}, *snooze button*^{p194}, *indecisive*^{p195}, and *late responder*^{p196} mutants, while *biased*^{dp197} and *fashionably late*^{p191} mutants displayed mildly increased and decreased levels of spontaneous movement, respectively (Table 1). No mutants displayed deficits in habituating to repeated acoustic stimuli (Table 1), highlighting that simple learning and decision-making processes are genetically separable. Similarly, responsiveness to visual (dark-flash) stimuli was normal in all mutants. While *snooze button*^{p194} and *better late than never*^{p193} had shorter and longer visually evoked response latencies, respectively, the remaining mutants were indistinguishable from their siblings (Table 1), underscoring the overall specificity of the behavioral screen for acoustic sensorimotor decision making.

To determine whether the identified mutants indeed affect sensorimotor decision making, we focused on the *wrong turn* mutant, because of its consistently strong phenotype (Figure 2B; Video S3). While wild-type larvae dynamically shift from LLC to SLC responses with increasing stimulus intensities, *wrong turn* mutants exhibited a strong bias toward LLC behaviors at all stimulus intensities (Figures 1C and 2D). Moreover, *wrong turn* mutants display largely normal or mildly elevated overall responsiveness to acoustic stimuli, despite their bias toward LLC responses (Figure 2E), consistent with sensory acuity being largely unaffected in *wrong turn* mutants. We then tested whether prior experience would affect behavioral selection in these mutants, examining whether they would shift their behavioral bias across repeated (1-s inter-stimulus interval [ISI]) identical acoustic stimuli. While wild-type larvae rapidly shift their bias from SLC to LLC responses following repeated strong stimuli, *wrong turn* mutant fish maintain a bias toward LLC responses across repeated stimuli (Figure 2F). Though they do not shift

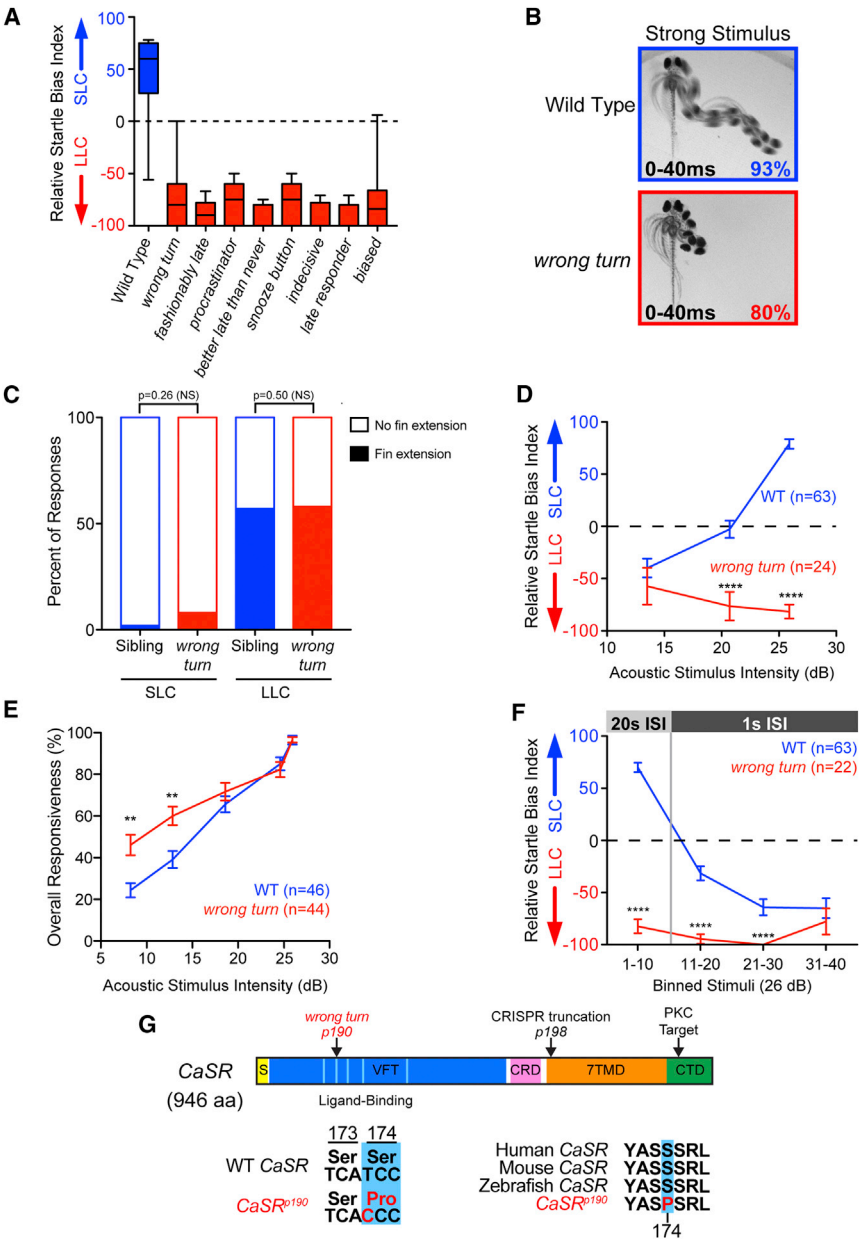

Figure 2. Isolation of Decision-Making Mutants from a Forward Genetic Screen

(A) Average startle biases of decision-making mutants, presenting the average bias of the "bottom 25%" of all tested larvae from heterozygous mutant carrier incrosses ($n \geqslant 47$ mutant larvae each), with the bottom 25% of representative wild-type larvae (Tüpfel long fin [TLF], indicated in blue; n = 28).

(B) Temporal projection over 40 ms post-stimulus (26 dB) of wild-type and *wrong turn* mutant 5-dpf larval responses. Percentage indicates average frequency observed (30 WT and 58 *wrong turn* larvae).

(C) Percentage of short- and long-latency responses using pectoral fins during the initial C-bend. n = 14 sibling (blue, 250 responses), and n = 14 *wrong turn* (red, 112 responses), Fisher's exact test.

(D and E) Acoustic stimulus intensity versus average relative startle index (D) or average overall startle responsiveness (E) for wild-type (blue) and *wrong turn* mutants (red).

(F) Average relative startle bias of 5-dpf *wrong turn* and wild-type larvae following identical 26-dB stimuli at 20-s intervals (stimuli 1–10) and then 1–s intervals (stimuli 11–40).

(G) Zebrafish CaSR protein showing locations of the *wrong turn*^{p190} and *CaSR*^{p198} mutations, Signal Sequence (S, yellow), extracellular Venus Fly Trap domain (VFT, blue), cysteine-rich domain (CRD, pink), 7-pass transmembrane domain (7TMD, orange), C-terminal domain (CTD, green), 5 key residues of the ligand-binding pocket of the VFT hinge (light blue), and PKC phosphorylation residue (arrowhead).

Error bars indicate SEM. **p < 0.01; ****p < 0.0001, Bonferroni-corrected t test. NS, not significant. See also Figures S3 and S4.

bias, mutant larvae are still able to reduce their responsiveness through this experience at levels similar to those of their siblings, indicating their mechanisms for acoustic startle habituation remain intact (Table 1). To exclude the possibility that the *wrong turn* mutation simply increases startle response latency, we compared the kinematic profiles of *wrong turn* short- and long-latency responses to those of sibling SLC and LLC behaviors. Overall, initial turn latencies, durations, maximal turning angles, and maximal angular velocities of the long-latency responses of *wrong turn* mutants resembled the parameters of sibling LLC responses, and all were significantly distinct from sibling SLC responses (Figure S3). Similarly, short-latency responses of *wrong turn* mutants kinematically resembled sibling SLC responses, not LLC responses (Figure S3). Furthermore, *wrong turn* mutants used their pectoral fins extensively during long-latency responses and rarely during short-latency responses, just like their siblings (Figure 2C). Finally, to exclude that the *wrong turn* mutant phenotype is caused by delayed neural circuit development, we examined 21-dpf juvenile *wrong turn* mutants, observing the same dramatic deficit in SLC versus LLC behavioral choice (Figures S3E and S3F). Combined, these results reveal a novel set of genetic mutations that selectively modulate SLC versus LLC behavioral choice and identify the *wrong turn* gene to be critical for sensorimotor decision making.

The G-Protein-Coupled Receptor CaSR Regulates Acoustic Decision Making

The eight decision-making mutants isolated provide unique entry points to determine how sensorimotor decision making in zebrafish is molecularly regulated. We focused on the *wrong turn* mutant to identify the causative molecular lesion via a whole-genome sequencing approach [24]. We first identified genomic regions of high homozygosity in a pool of behaviorally

Table 1. Behavioral Characterization of Decision-Making Mutant Larvae

Mutant Allele	Relative Bias (26 dB)	Total Response % (26 dB)	Relative Bias (13 dB)	Spontaneous Activity (Pixels/Second)	Acoustic Startle Habituation	Visual (Dark Flash) Response Latency (ms)	Complementing Alleles
wrong turn p190 (CaSR)	−75 ± 4 (n = 58)	93 ± 1 (versus 98, $p < 10^{-2}$)	−57 ± 18 (versus −41, p = 0.54)	55 ± 5 (versus 51, p < 0.97)	68% ± 6 (versus 72%, p < 0.66)	366 ± 23 (versus 330, p = 0.16)	*p191*, *p192*, *p196*
fashionably late p191	−72 ± 3 (n = 69)	77 ± 3 (versus 96, $p < 10^{-7}$)	−83 ± 10 (versus −58, p = 0.09)	20 ± 1 (versus 27, $p < 10^{-5}$)	56% ± 7 (versus 41%, p < 0.06)	ND	*p190*, *p192*, *p193*
procrastinator p192	−30 ± 4 (n = 58)	84 ± 4 (versus 94, $p < 10^{-3}$)	−97 ± 3 (versus −46, $p < 10^{-4}$)	30 ± 1 (versus 27, p < 0.10)	70%±5 (versus 72%, p < 0.74)	198 ± 7 (versus 188, p = 0.29)	*p190*, *p191*
better late than never p193	−93 ± 1 (n = 65)	67 ± 4 (versus 77, p < 0.11)	−57 ± 8 (versus −52, p = 0.75)	37 ± 1 (versus 39, p < 0.26)	94% ± 2 (versus 94%, p < 0.95)	270 ± 7 (versus 246, p = 0.019)	*p191*
snooze button p194	−40 ± 4 (n = 74)	83 ± 3 (versus 96, $p < 10^{-4}$)	−33 ± 18 (versus −36, p = 0.90)	24 ± 1 (versus 24, p < 0.64)	92% ± 3 (versus 79%, p < 0.0005)	244 ± 23 (versus 327, p = 0.0033)	*p195*
indecisive p195	−23 ± 5 (n = 88)	90 ± 2 (versus 98, $p < 10^{-5}$)	−70 ± 11 (versus −54, p = 0.27)	22 ± 1 (versus 23, p < 0.68)	86% ± 2 (versus 90%, p < 0.12)	255 ± 18 (versus 269, p = 0.51)	*p194*
late responder p196	−71 ± 3 (n = 59)	82 ± 3 (versus 95, $p < 10^{-3}$)	−98 ± 2 (versus −45, $p < 10^{-4}$)	22 ± 2 (versus 26, p < 0.10)	69% ± 4 (versus 71%, p < 0.63)	275 ± 10 (versus 270, p = 0.72)	*p190*
biased dp197	−49 ± 5 (n = 83)	85 ± 2 (versus 98, $p < 10^{-6}$)	−76 ± 9 (versus 66, $p < 10^{-14}$)	36 ± 1 (versus 31, p < 0.011)	87% ± 4 (versus 86%, p < 0.92)	201 ± 6 (versus 189, p = 0.22)	ND

Mean values ± SEM for each assay on 5- to 6-dpf larvae; significance was determined by t test (see STAR Methods). ND, not determined.

selected *wrong turn* mutants and then verified linkage to an 800-kb region of chromosome 5 through bulked segregant analysis (Figure S4A) [24, 26]. Within this genomic region, we identified a T-to-C nucleotide change that strongly segregated with the *wrong turn* phenotype and was absent in over 257 reads of related wild-type control samples. This mutation changed amino acid 174 from a serine to a proline in the coding sequence of the extracellular *CaSR* (Figure 2G). CaSR is a G-protein-coupled receptor (GPCR) that detects alterations in extracellular calcium concentrations, best known for its critical role in modulating parathyroid hormone secretion and urinary calcium excretion [27]. Though expressed in the vertebrate CNS (Figure S5A), CaSR's function in the nervous system is not well understood [28–30].

The serine residue mutated in *wrong turn* is conserved across vertebrate *CaSR* orthologs (Figure 2G) and is a key residue in the hinge region of the extracellular domain critical for full CaSR activity [31], suggesting that the mutation disrupts CaSR's calcium-sensing function. To confirm that mutations in *CaSR* cause the *wrong turn* behavioral phenotype, we generated a 7-bp deletion in *CaSR*, causing a premature stop codon in the first transmembrane domain at position 613 of the *CaSR* protein ($CaSR^{p198}$; Figures 2G and S4B). Trans-heterozygous larvae carrying both *wrong turn* and the new $CaSR^{p198}$ allele exhibited the same behavior selection defect when exposed to intense stimuli, exhibiting a strong inappropriate bias toward LLC behaviors (Figure S4C). These data confirm that mutations in *CaSR* cause the *wrong turn* behavioral deficits and identify *CaSR* as a critical regulator of sensorimotor decision making.

In cultured neurons, CaSR can regulate neuronal morphology through neurite outgrowth [29] as well as neuronal activity and synaptic release [32, 33]. Given the striking decrease in SLC response selection by *CaSR* mutants, we first examined the morphology of the Mauthner command neuron, which is essential to elicit SLC behavior [15, 34–36]. Using a transgenic line expressing membrane-targeted citrine in Mauthner neurons, we measured the volume and surface area of the lateral and ventral dendrites receiving acoustic and visual inputs, respectively, as well as of the initial axon segment (IAS) receiving input from spiral fiber neurons and of the remaining Mauthner soma (Figures 3A and 3B) [24]. The volume and surface area of the axonal initial segment, and both ventral and lateral dendrites, were indistinguishable between *CaSR* mutants and wild-type siblings (Figures 3C and 3D). However, *CaSR* mutants exhibited a mild increase in soma surface area without an increase in volume, suggesting a possible impact on Mauthner cell function (Figures 3C and 3D).

To test whether Mauthner neuronal function requires *CaSR*, we examined wild-type and *CaSR* mutant Mauthner function through GCaMP6s calcium imaging and electrophysiological recordings. In wild-type siblings, short-latency startles were strongly associated with a robust calcium response in the Mauthner soma (Figures 3E, 3F, and 3K), while minimal change was detected when long-latency startles were performed, consistent with published results (Figures 3G and 3K) [37]. *CaSR* mutant Mauthner soma showed a similar strong calcium response when short-latency startles were performed (Figures 3H, 3I, and 3K). Similarly, when long-latency startles were performed, the calcium responses of *CaSR* mutant Mauthner soma were indistinguishable from those of their siblings (Figures 3J and 3K). We further investigated whether changes in the excitability of the Mauthner neurons could explain or contribute to the behavioral phenotype of *CaSR* mutant fish through electrophysiological recordings. Whole-cell recordings revealed no alteration in the rheobase (amount of current necessary to trigger an action potential), resting potential ($V_{resting}$), or input resistance (R_{in}) of *CaSR* mutant Mauthner neurons (Table S2). Though we observed a small increase in the Mauthner membrane

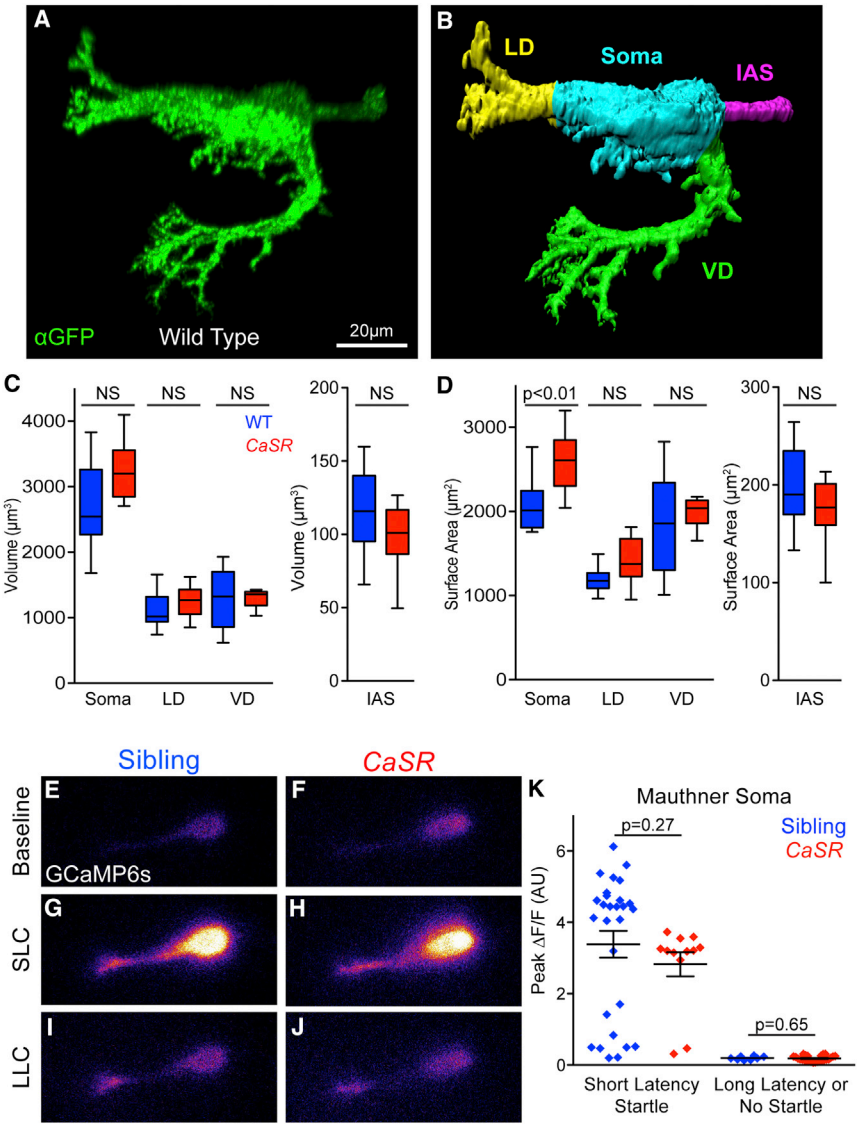

Figure 3. Mauthner Morphology and Function Are Largely Unperturbed in *CaSR* Mutants

(A) Representative projection of wild-type Mauthner-neuron-expressing membrane-targeted gap43-citrine, stained with anti-GFP. Non-Mauthner labeling was thresholded, and neurons were reoriented for clarity.

(B) Surface of wild-type Mauthner neuron from (A) segmented into the lateral dendrite (LD, yellow), ventral dendrite (VD, green), initial axon segment (IAS, magenta), and soma (cyan) for morphological quantification.

(C and D) Quantification of the volume (C) and surface area (D) of segmented Mauthner neuron regions (n = 15 sibling and 12 *CaSR* mutant neurons).

(E–J) Representative GCaMP6s fluorescence in Mauthner neurons of sibling (E, G, and I) and *CaSR* mutant (F, H, and J) larvae. Baseline fluorescence immediately prior to stimuli (E and F), and peak fluorescence during SLC (G and H) or LLC (I and J).

(K) Peak ΔF/F in Mauthner soma during responses of sibling (blue) and *CaSR* mutant (red) larvae to 13-dB acoustic stimuli. n = 28 sibling SLC responses, 12 *CaSR* SLC responses, 8 sibling LLC responses, and 26 *CaSR* LLC responses.

Error bars indicate SEM. See also Figure S5 and Table S2.

potential threshold for action potential generation ($V_{Threshold}$, +4.6 mV in mutants), this difference alone does not represent a relevant modification of Mauthner neuron excitability, and over one-third of mutant Mauthners had a $V_{Threshold}$ within the range of wild-type variation, despite their strong behavioral phenotype.

We next explored whether *CaSR* might be required for appropriate excitatory input to the Mauthner neuron, examining the role of the lateral line sensory organ, the distribution of electrical synapses important for Mauthner activation, and the level of excitatory calcium influx at the lateral dendrite. *CaSR* is expressed in the neuromasts of the lateral line sensory organ [38], so we reasoned that if *CaSR* regulates response selection here, then disrupting the lateral line sensory input should impair larval decision making. After ablating the sensory hair cells of the lateral line with neomycin, we observed no significant change in behavioral selection at any stimulus intensity tested (4.6–25.9 dB), indicating that CaSR is unlikely to impact behavioral selection at the level of sensory input from the lateral line organ (Figure S5F). Next, we examined the distribution of Connexin 35/36 on the Mauthner cell surface to determine whether developmental assembly or maintenance of the major excitatory synaptic connections to the Mauthner requires *CaSR*. In wild-type animals, Connexin 35/36 immunoreactivity is enriched at large club-ending synapses that transmit acoustically evoked excitatory inputs to the lateral dendrite of the Mauthner neurons from the VIIIth statoacoustic nerve, as well as at electrical synapses between spiral fiber neurons that provide excitatory input to the Mauthner initial axonal segment [39]. We observed no significant difference in the levels, localization, or number of Connexin 35/36 puncta in *CaSR* mutants compared to wild-type siblings (Figure S5). Finally, we monitored GCaMP6s fluorescence in the Mauthner lateral dendrite in response to weak subthreshold acoustic stimuli to determine whether excitatory calcium influx was altered in the dendrite. *CaSR* mutant and sibling larvae both showed similar dendritic activity in response to weak stimulation, arguing against a role for CaSR in Mauthner dendritic excitation (Figure S5G). Thus, while Mauthner neurons in *CaSR* mutants exhibit a mild increase in soma surface area and $V_{Threshold}$, the structure of major excitatory synaptic inputs as well as Mauthner activity during SLC and LLC responses are indistinguishable from those in wild-type siblings, providing compelling evidence that, instead of mediating SLC responses, CaSR regulates the behavioral choice between SLC and LLC.

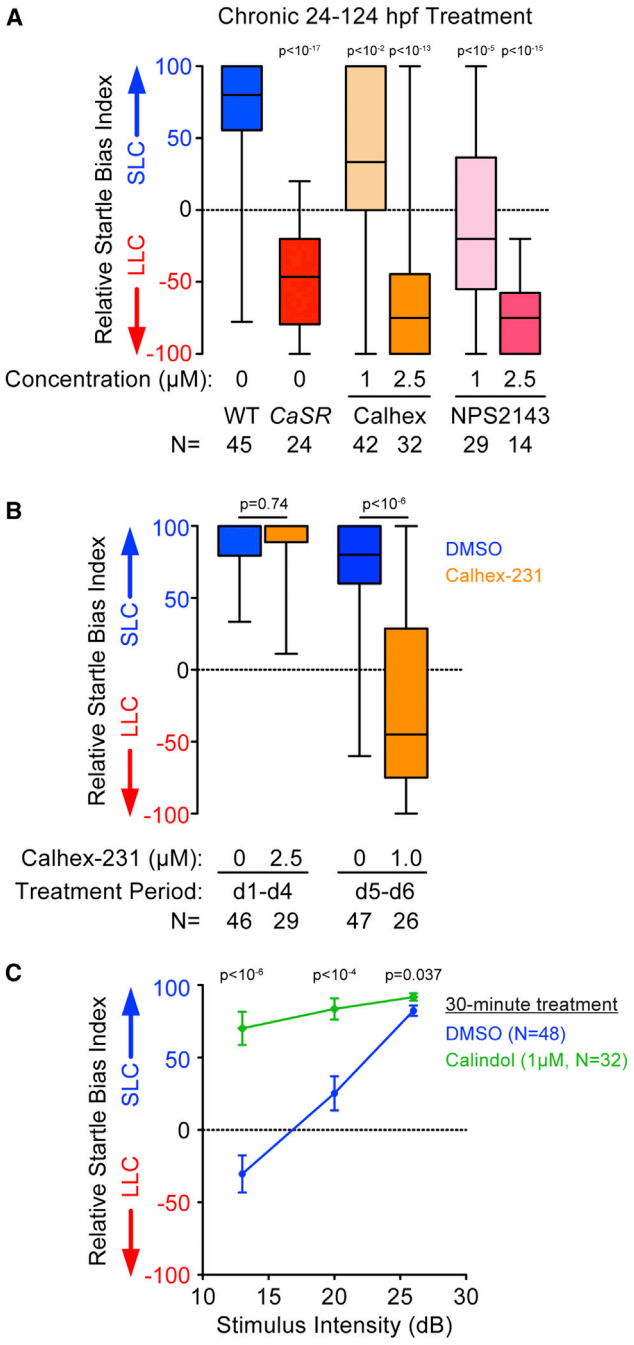

Figure 4. Pharmacological Modulation of CaSR Activity Regulates Acoustic Decision Making

(A) Chronic treatment (24–124 hpf) with CaSR antagonists Calhex-231 and NPS2143 shifts average decision-making bias of wild-type larvae toward LLC behavior.

(B) Relative startle bias of 6-dpf larvae following exposure to CaSR antagonist Calhex during circuit development (24–112 hpf) or post-circuit development (120–144 hpf).

(C) Decision-making bias of 5-dpf larvae following 30-min acute activation of CaSR with 1 μM calindol.

Error bars indicate SEM; Bonferroni-corrected t test versus DMSO control. See also Figure S6.

CaSR Acutely Regulates Acoustic Decision Making

We next tested whether CaSR regulates sensorimotor decision making during development, e.g., by establishing neural circuitry, or acutely, e.g., by modulating neural activity. For this, we first treated wild-type individuals with two well-characterized CaSR antagonists (Calhex-231 or NPS2143 [40]), from 24 hpf through 124 hpf, and then tested their acoustic response bias. Whereas control DMSO-treated larvae exhibited a strong bias toward SLC responses to intense (26-dB) stimuli, Calhex-231- or NPS2143-treated larvae displayed dose-dependent changes in response bias to favor LLC responses, similar to *CaSR* mutant larvae (Figure 4A). We then restricted the period of CaSR antagonist treatment to distinguish between CaSR's roles in circuit development or function. Exposing larvae to CaSR antagonists during the period of circuit development (between 24 and 112 hpf) did not alter acoustic response bias (Figure 4B). In contrast, exposing larvae to CaSR antagonists only after the main period of circuit development (between 120 and 144 hpf) fully recapitulated the behavioral bias deficits observed in *CaSR* mutants (Figure 4B). Conversely, acutely exposing larvae to the CaSR agonist calindol for 30 min [41] significantly shifted larval behavioral bias toward SLC responses to low-intensity stimuli (Figure 4C). While these CaSR modulators were also capable of affecting total larval responsiveness, under conditions with little-to-no responsiveness change, we still observe clear significant shifts to acoustic response bias (Figures S6A–S6C). Thus, CaSR activity acutely and bidirectionally regulates acoustic decision making.

CaSR Functions as a Canonical GPCR to Regulate Decision Making

CaSR has been shown to act by signaling through several G-proteins, including $G\alpha_{i/o}$, $G\alpha_{s}$, and $G\alpha_{q/11}$, depending on the cell type, environment, and developmental status of the tissue (Figure 5A) [42]. CaSR activity can be regulated through clathrin-mediated endocytosis, which removes CaSR from the cell surface, thereby terminating its activity [43]. Given that CaSR signaling has been predominantly examined in non-neuronal tissues, we wondered whether CaSR regulates sensorimotor decision making through $G\alpha_{i/o}$, $G\alpha_{s}$, or $G\alpha_{q/11}$ and/or whether clathrin-dependent pathways modulate CaSR's function in neurons. CaSR activity can regulate intracellular cAMP levels through $G\alpha_{s}$-dependent activation of adenylyl cyclase (AC), increasing cAMP, or through $G\alpha_{i/o}$-dependent inhibition of AC, reducing cAMP [42, 44, 45]. To test whether either pathway modulates acoustic decision making *in vivo*, we pharmacologically increased cAMP levels in wild-type larvae and examined whether this shifted their behavioral bias. For this, we tested the behavioral bias of larvae exposed to intense acoustic stimuli in the presence of 2.5 μM forskolin to activate AC. While control larvae displayed a strong bias toward SLC responses, forskolin-dependent AC activation shifted response bias toward LLC performances (Figure 5B). Moreover, exposing larvae to the phosphodiesterase IV (PDE4) inhibitor rolipram to inhibit cAMP degradation also shifted larval response bias toward LLC performance (Figure 5B). While rolipram can also impact responsiveness to acoustic stimuli at these levels, forskolin has minimal impact on responsiveness under conditions where behavioral selection is strongly altered (Figures S6D and S6E). If forskolin

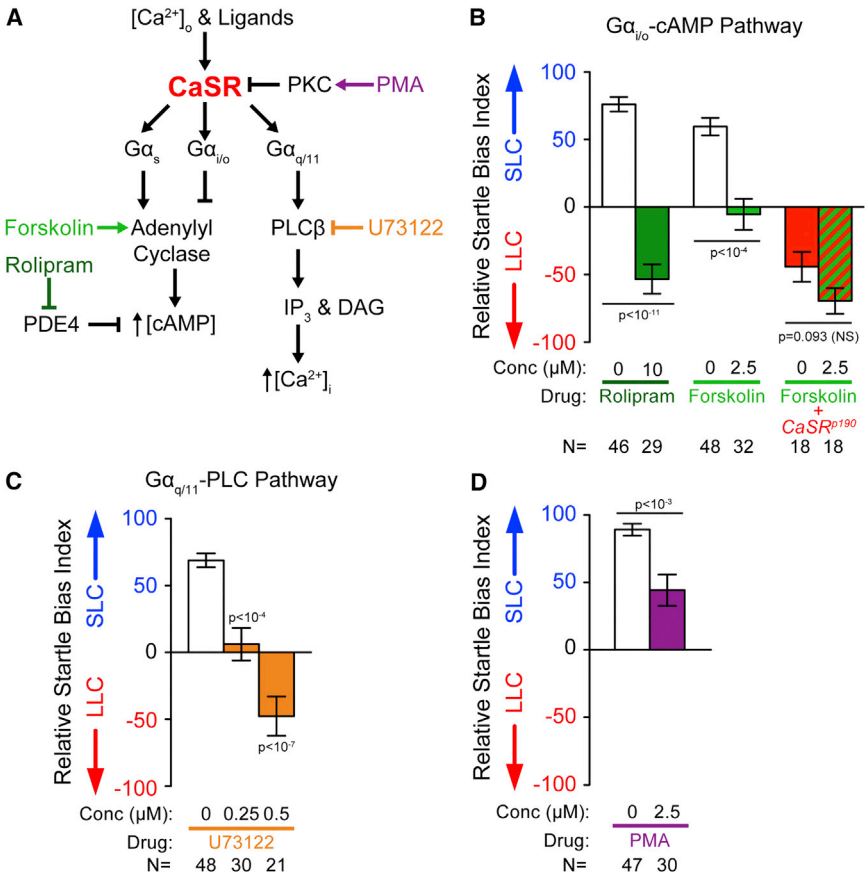

Figure 5. Molecular Pathways of CaSR Signaling and Regulation Control Acoustic Decision Making

(A) Molecular pathways implicated in CaSR signaling and regulation.

(B–D) Average startle bias index of 5-dpf larvae following 20-min acute drug treatments. Disruption of $G\alpha_{i/o}$/cAMP signaling produced with 10 μM rolipram or 2.5 μM forskolin (B), disruption of $G\alpha_{q/11}$ signaling produced with U73122 (C), and activation of PKC with phorbol 12-myristate 13-acetate (PMA) (D).

Error bars indicate SEM; significance was determined by Bonferroni-corrected t test versus DMSO control. See also Figure S6.

were shifting behavioral selection through an alternate signaling pathway, we might expect it to exacerbate the bias of *CaSR* mutants; however, this level of forskolin does not significantly impact the *CaSR* bias phenotype (Figure 5B). In sum, acutely elevating cAMP levels recapitulates CaSR deactivation (Figure 4B), consistent with the idea that CaSR modulates acoustic decision making—at least in part—via $G\alpha_{i/o}$ (Figure 5A).

CaSR also can signal through $G\alpha_q$ to activate phospholipase C β (PLCβ), which generates diacylglycerol (DAG) and inositol triphosphate (IP_3) to increase intracellular Ca^{2+} [46, 47]. To test whether this signaling pathway modulates acoustic decision making, we exposed larvae to PLCβ inhibitor U73122 for 20 min and then determined behavioral bias. While DMSO-treated larvae were strongly biased toward SLC responses, U73122 treatment produced an acute dose-dependent shift in response bias toward LLCs (Figure 5C), phenocopying CaSR deactivation. Similar to other CaSR signaling modulators, U73122 can also impact overall larval responsiveness to acoustic stimuli, though a strong shift in behavioral bias is observed even at low concentrations with minimal responsiveness alteration (0.25 μM U73122), arguing that the decision-making phenotype is a direct effect of the drug rather than a secondary consequence (Figures S6F and S6G). Finally, we acutely exposed wild-type larvae to protein kinase C (PKC) inhibitor phorbol 12-myristate 13-acetate (PMA), which impairs CaSR/$G\alpha_{q/11}$ signaling-dependent intracellular Ca^{2+} increase in cell culture [48]. Acute exposure to 2.5 μM PMA shifted the bias of larvae toward LLC responses, supporting a role for PKC-dependent modulation of bias (Figure 5D) and further supporting the idea that CaSR signaling via $G\alpha_q$ modulates acoustic decision making.

Finally, we tested whether CaSR-dependent decision making is also regulated by clathrin-mediated endocytosis. Specifically, the Adaptor Protein 2 (AP2) complex facilitates CaSR internalization from the plasma membrane by clathrin-mediated endocytosis, and mutations in both *CaSR* and the AP2 complex σ subunit (*AP2S1*) cause human hypercalcemia [49–51]. To determine whether the AP2 complex plays a role in CaSR-dependent decision making, we first examined acoustic startle bias in *ap2s1* mutants that we isolated in a companion screen for startle modulation (Figures 6A and S7) [24]. We found that *ap2s1* mutants showed a strong bias toward SLC responses, regardless of stimulus intensity (Figure 6B). Combined with the functional interaction between CaSR and AP2σ in cell culture [50], this suggested that *ap2s1* regulates sensorimotor decision making by removing CaSR from the cell surface and, hence, terminating CaSR activity. This model predicts that partially reducing *ap2s1* and CaSR function simultaneously should ameliorate the LLC-shifted bias observed in *CaSR* mutants. Indeed, in response to strong (25.9-dB) stimuli when *CaSR* mutants inappropriately selected LLC behaviors, *CaSR; ap2s1* double mutants showed significant rescue of their bias back toward SLC behavior (Figure 6C). Combined these data support the model that *CaSR* promotes sensorimotor decision making acutely through $G\alpha_{i/o}$ and $G\alpha_{q/11}$ signaling and that CaSR signaling is likely modulated via clathrin-mediated endocytosis.

DISCUSSION

Selecting the most appropriate response from a pre-existing behavioral repertoire is crucial for individuals to successfully navigate their environment. Here, we show that zebrafish larvae prioritize behavioral responses to acoustic stimuli with several key behavioral and pharmacological characteristics of dynamic decision making in other animals [21, 22]. Through a forward

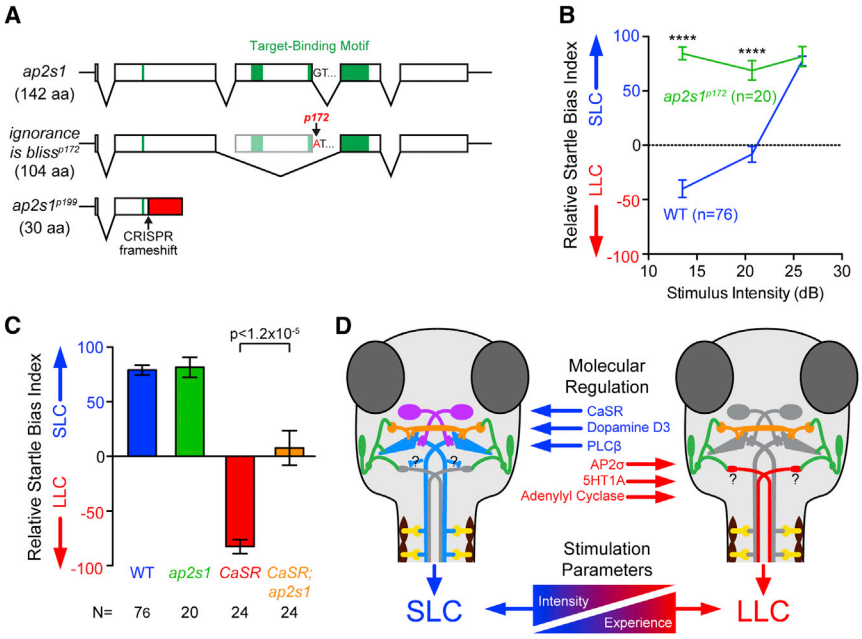

Figure 6. AP2σ Modulates CaSR-Dependent Acoustic Decision Making

(A) Diagram of *ap2s1* alleles and motifs.

(B) Average relative startle bias of *ap2s1*^{p172} mutants. ****p < 0.0001.

(C) Average relative startle bias of 5-dpf wild-type, *ap2s1*^{p172}, *CaSR*^{p190}, and *CaSR*^{p190};*ap2s1*^{p172} double-mutant larvae at 25.9 dB.

(D) General model of acoustic sensorimotor decisionmaking: green indicates hair cells and VIIIth statoacoustic nerve, blue indicates Mauthner neurons, violet indicates spiral fiber neurons, orange indicates feed-forward PHP inhibitory neurons, yellow indicates spinal motor neurons, and red indicates proposed LLC command neurons. Error bars indicate SEM; significance was determined by t test. See also Figure S7.

genetic screen, we identified a first set of genes underlying sensorimotor decision making, including the vertebrate-specific GPCR *CaSR*. *CaSR* function is required to modulate response bias based on stimulus quality and history, two hallmarks of sensorimotor decision making. Rather than regulating the execution of SLC or LLC behaviors, *CaSR* acts acutely in the selection process that enables larvae to prioritize SLC over LLC responses.

Zebrafish Larvae Exhibit Robust Sensorimotor Decision Making

Using a combination of behavioral and pharmacological experiments, we find that zebrafish larvae prioritize behavioral responses to acoustic stimuli with several key hallmarks of dynamic decision making [21, 22]. First, at 5 dpf, zebrafish larvae already possess the ability to select between the kinematically and neuronally distinct SLC and LLC behaviors evoked by the same stimuli. Response speed is critical for predator evasion in zebrafish and other small fish [52, 53], and unlike SLC responses, LLC responses produce minimal body displacement within 40 ms of acoustic stimuli, perhaps more consistent with a re-orientation behavior to evaluate non-threatening stimuli (Figure 1B). Thus, LLC behavior is poorly suited for escape from likely fast-striking aquatic predators [54], and selection of the appropriate acoustic response is likely an ethologically relevant decision [55]. Second, the response selection mechanism is driven by stimulus quality, as larvae predictably shift their response bias from LLC to SLC behavior with increasing stimulus intensity rather than using stochastic or fixed reflexive behavior selection mechanisms. Third, response selection is modulated and informed by prior experience. Though the acoustic responses examined here initiate on the order of 4–80 ms, we demonstrate that behavioral response selection is carefully modulated and informed by experience accumulated over the course of several seconds (Figure 1D) [23]. Multiple modalities are integrated in the impact of this prior experience, as repeated inconsequential acoustic stimuli shift bias toward LLC behavior (Figure 1D), while exposure to tactile stimuli or visual stimuli can enhance subsequent SLC selection [23, 56]. Finally, acoustic behavior selection is modulated by serotonin and dopamine, conserved modulators of decision-making and behavioral bias from invertebrates to humans [57, 58]. Thus, LLC versus SLC response bias represents a quantifiable and high-throughput behavioral choice paradigm sharing key characteristics of more complex decision making.

The Role of CaSR in Controlling Behavioral Bias

Using the observer independent and high-throughput behavioral paradigm outlined earlier, we conducted the first genetic screen for genes critical for vertebrate decision making. We demonstrate that the mutants we identified from this screen are all still capable of performing both SLC and LLC behaviors, so rather than merely disrupting performance of particular motor patterns, instead, they reveal the genetic blueprint underlying the behavioral selection process itself (Figure 2A). Whole-genome sequencing revealed an unexpected yet key role for *CaSR* in sensorimotor decision making. CaSR has been extensively studied for its role in regulating parathyroid hormone secretion and serum calcium levels, with inactivating and activating *CaSR* mutations causing hypercalcemia or hypocalcemia in humans, respectively [27]. Defects of the nervous system and behavior have also been observed in humans with *CaSR* disruptions, including mental retardation, dementia, and epilepsy [59–61]. However, the extent to which these neural deficits are due to direct neuronal functions of CaSR or secondary effects of hormonal secretion or serum ion composition changes has been unclear. The Ser-174 residue mutated in *CaSR*^{p190} corresponds to the Ser-170 residue of human CaSR, and when mutated in cultured cells, this strongly decreases CaSR signaling activity [31, 62]. CaSR crystal structures indicate that this residue is located in a ligand-binding pocket for extracellular aromatic amino acids and/or Ca^{2+} ions critical for CaSR activity and signaling [63, 64]. Thus, combined with the behavioral phenocopy produced by CaSR antagonists, the *CaSR*^{p190} mutation likely disrupts its ability to monitor and respond to a variety of

extracellular molecular signals to modulate decision-making behavior.

CaSR mutant mice show both direct and indirect (hormonal) defects in brain development, neural proliferation, and neuronal morphology in culture [29, 65]. Treating zebrafish larvae with pharmacological CaSR modulators revealed a direct and acute role for CaSR in modulating sensorimotor decision making (Figure 4). Moreover, acutely increasing or decreasing CaSR activity shifted behavioral bias in opposing directions, suggesting that, rather than regulating a single-circuit component/connection in an on/off manner, *CaSR* modulates the behavioral balance between SLC and LLC behaviors at several levels; for example, by acting presynaptically and/or postsynaptically. Indeed, CaSR protein localizes to synapses [66], and presynaptic CaSR activation reduces glutamate release in cultured neurons through regulation of presynaptic cation channels [32]. Postsynaptically, CaSR activity modulates K+ channel activity and nonselective cation channels to regulate their excitability [33, 67]. Paradoxically, CaSR can also enhance spontaneous release of both GABA and glutamate, which might support homeostatic plasticity and/or synaptic facilitation [33, 67–69]. Finally, CaSR also forms functional heterodimers with neurotransmitter receptors, including GABA-B type, mGluR1, and mGluR5 receptors in neurons [70, 71]; thus, CaSR might also modulate responses to these associated neurotransmitters in sensorimotor decision-making circuits.

How then does CaSR regulate SLC versus LLC behavioral bias? Our data and previously published work support a model where acoustic stimuli can activate competing hindbrain escape circuits that drive SLC or LLC behavior [15, 72, 73]. Modulation by high CaSR activity, dopaminergic signaling through D3, and PLCβ activity would promote SLC circuit activity, while low CaSR activity, serotonergic signaling through 5HT1A, and increased AC activity would, instead, favor activation of the LLC-driving circuitry (Figure 6D). Given the mutant and pharmacological phenotypes observed, normal CaSR activity is predicted to relieve inhibition onto the Mauthner neuron while also enhancing excitatory drive on the Mauthner neurons and/or dampening excitation of LLC command-like neurons. To regulate Mauthner inhibition, CaSR could act in feed-forward passive hyperpolarizing (PHP) neurons to reduce glycine release at synapses on the Mauthner neuron or at the synapse between the VIIIth statoacoustic nerve and feed-forward PHP neurons, presynaptically reducing glutamate release or postsynaptically hyperpolarizing the PHP neurons [16, 74, 75]. Disrupting CaSR function would therefore increase PHP activity, oversilencing the Mauthner neurons and permitting the LLC circuit to dominate. CaSR could enhance Mauthner excitation by depressing inhibitory neurotransmission onto the spiral fiber neurons that receive indirect input from the auditory nerve and enhance Mauthner activity, as ablation of spiral fiber neurons produces a shift in SLC/LLC bias similar to *CaSR* mutants [19]. Though we observed mild increases in Mauthner surface area and $V_{Threshold}$, these did not impact Mauthner input resistance or excitability, and given the acute (30-min) impact of pharmacological CaSR activation on behavior selection, neuronal morphology change is unlikely to be the primary role for CaSR in this process. Finally, CaSR could also act at the excitatory synapse on the predicted LLC command neurons to limit the excitation or response of these neurons; thus, CaSR disruption would increase the activity of these neurons to promote LLC behaviors. However, for this to be the primary site of CaSR, action would also require a mechanism where Mauthner activity is inhibited by an activated LLC circuit, which is unlikely, given the extremely short latency from stimulus to Mauthner activation. *CaSR* is expressed broadly throughout the zebrafish brain (Figure S5A) [28]; thus, determining the neuronal cell population in which *CaSR* is required for SLC versus LLC choice will narrow down the potential mechanisms of how *CaSR* modulates the acoustic decision-making process and reveal the neurons critical for this behavioral selection.

Circuit Control of Sensorimotor Decision Making

Similar to zebrafish, *Drosophila* exhibit two related escape responses, a ''short mode'' jump response with short latency driven by descending Giant Fiber neurons and a more controlled ''long mode'' response with a longer latency involving coordinated wing movements and finer directional control driven through Giant-Fiber-independent descending circuits [76]. The Giant Fiber circuit has a higher activation threshold than the parallel ''long mode'' circuit and can override ''long mode'' behavior to force a short takeoff. Thus, the relative timing of Giant Fiber versus non-Giant Fiber activation drives escape behavior selection. It is tempting to speculate that a similar mechanism biases SLC versus LLC behavior selection in zebrafish. Indeed, similar to the Giant-Fiber-driven escape in *Drosophila*, zebrafish SLC behavior is an ''all-or-nothing'' response, with stereotyped kinematic parameters regardless of stimulus quality, while LLC speed, angle, and latency are informed by the intensity of the stimulus to allow greater directional control [15]. Furthermore, Mauthner firing in goldfish activates and silences arrays of hindbrain reticulospinal neurons [77]. Given the differences in latency, Mauthner activity might actively prevent and preempt activation of the LLC circuit (Figure 6D). For example, Mauthner neurons and MiD3cm reticulospinal neurons display complementary activity patterns that correlate with short- and long-latency responses to water pulses [72], making MiD3cm neurons candidate neurons for controlling acoustically evoked LLC behavior. Goldfish MiD3cm neurons show a 10-fold lower activation threshold than Mauthner neurons and fire with longer latency than Mauthner neurons in response to strong VIIIth statoacoustic nerve activation [17], consistent with the relative timing mechanism underlying *Drosophila* escape selection. Future experiments using whole-brain imaging techniques in zebrafish are required to identify both the neurons driving LLC behavior and those impacting SLC versus LLC selection, and it will be of great interest to determine the degree of conservation in the sensorimotor decision-making mechanisms underlying ethologically relevant escape behaviors.

STAR★METHODS

Detailed methods are provided in the online version of this paper and include the following:

- KEY RESOURCES TABLE
- CONTACT FOR REAGENT AND RESOURCE SHARING
- EXPERIMENTAL MODEL AND SUBJECT DETAILS

SUPPLEMENTAL INFORMATION

Supplemental Information includes seven figures, three tables, and three videos and can be found with this article online at https://doi.org/10.1016/j.cub.2018.03.025.

ACKNOWLEDGMENTS

The authors thank Dr. Mary Mullins, Dr. Shannon Fisher, Mr. Bill Vought, and Ms. Paula Roy for help with the genetic screen; Ms. Jessica Keel, Dr. Laura Liss, and Dr. Lauren Schmidt for help with the chemical screen; and Drs. Koichi Kawakami and Jon Raper for providing the *Tg(GFFDMC130A)* and *Tg(UAS:gap43-citrine)* fish, respectively. We also thank the Granato and Jain lab members for advice on the manuscript. This work was supported by NIH grants to R.A.J. (F32NS065637), A.E.P. (R01DC011099), and M.G. (R01MH092257 and R01MH109498).

AUTHOR CONTRIBUTIONS

R.A.J., M.A.W., K.C.M., and M.G. designed the research; R.A.J., M.A.W., K.C.M., J.C.N., H.S., F.A.E., C.S., H.B., J.S., E.N.C., K.S., and A.D.Z. performed research; R.A.J., M.A.W., K.C.M., J.C.N., H.S., F.A.E., C.S., and A.E.P. analyzed data; R.A.J. and M.G. wrote the paper.

DECLARATION OF INTERESTS

The authors declare no competing interests.

Received: August 25, 2017
Revised: January 24, 2018
Accepted: March 13, 2018
Published: April 19, 2018

REFERENCES

1. Eaton, R.C., ed. (1984). Neural Mechanisms of Startle Behavior (Springer).
2. Sillar, K.T., Picton, L.D., and Heitler, W.J. (2016). The Neuroethology of Predation and Escape (John Wiley & Sons).
3. Lima, S.L., and Dill, L.M. (1990). Behavioral decisions made under the risk of predation: a review and prospectus. Can. J. Zool. *68*, 619–640.
4. Palmer, C.R., and Kristan, W.B., Jr. (2011). Contextual modulation of behavioral choice. Curr. Opin. Neurobiol. *21*, 520–526.
5. Gold, J.I., and Shadlen, M.N. (2007). The neural basis of decision making. Annu. Rev. Neurosci. *30*, 535–574.
6. Korn, H., and Faber, D.S. (2005). The Mauthner cell half a century later: a neurobiological model for decision-making? Neuron *47*, 13–28.
7. Kristan, W.B. (2008). Neuronal decision-making circuits. Curr. Biol. *18*, R928–R932.
8. Wolpert, D.M., and Landy, M.S. (2012). Motor control is decision-making. Curr. Opin. Neurobiol. *22*, 996–1003.
9. Doya, K., and Shadlen, M.N. (2012). Decision making. Curr. Opin. Neurobiol. *22*, 911–913.
10. Glimcher, P.W. (2003). Decisions, Uncertainty, and the Brain: the Science of Neuroeconomics (MIT Press).
11. Kawano, T., Po, M.D., Gao, S., Leung, G., Ryu, W.S., and Zhen, M. (2011). An imbalancing act: gap junctions reduce the backward motor circuit activity to bias *C. elegans* for forward locomotion. Neuron *72*, 572–586.
12. Jovanic, T., Schneider-Mizell, C.M., Shao, M., Masson, J.-B., Denisov, G., Fetter, R.D., Mensh, B.D., Truman, J.W., Cardona, A., and Zlatic, M. (2016). Competitive disinhibition mediates behavioral choice and sequences in *Drosophila*. Cell *167*, 858–870.e19.
13. Barker, A.J., and Baier, H. (2015). Sensorimotor decision making in the zebrafish tectum. Curr. Biol. *25*, 2804–2814.
14. Korn, H., and Faber, D.S. (1996). Escape behavior - brainstem and spinal cord circuitry and function. Curr. Opin. Neurobiol. *6*, 826–832.
15. Burgess, H.A., and Granato, M. (2007). Sensorimotor gating in larval zebrafish. J. Neurosci. *27*, 4984–4994.
16. Hatta, K., and Korn, H. (1998). Physiological properties of the Mauthner system in the adult zebrafish. J. Comp. Neurol. *395*, 493–509.
17. Nakayama, H., and Oda, Y. (2004). Common sensory inputs and differential excitability of segmentally homologous reticulospinal neurons in the hindbrain. J. Neurosci. *24*, 3199–3209.
18. Pujol-Martí, J., and López-Schier, H. (2013). Developmental and architectural principles of the lateral-line neural map. Front. Neural Circuits *7*, 47.
19. Lacoste, A.M.B., Schoppik, D., Robson, D.N., Haesemeyer, M., Portugues, R., Li, J.M., Randlett, O., Wee, C.L., Engert, F., and Schier, A.F. (2015). A convergent and essential interneuron pathway for Mauthner-cell-mediated escapes. Curr. Biol. *25*, 1526–1534.
20. McClenahan, P., Troup, M., and Scott, E.K. (2012). Fin-tail coordination during escape and predatory behavior in larval zebrafish. PLoS ONE *7*, e32295.
21. Ernst, M., and Paulus, M.P. (2005). Neurobiology of decision making: a selective review from a neurocognitive and clinical perspective. Biol. Psychiatry *58*, 597–604.
22. Pearson, J.M., Watson, K.K., and Platt, M.L. (2014). Decision making: the neuroethological turn. Neuron *82*, 950–965.
23. Wolman, M.A., Jain, R.A., Liss, L., and Granato, M. (2011). Chemical modulation of memory formation in larval zebrafish. Proc. Natl. Acad. Sci. USA *108*, 15468–15473.
24. Wolman, M.A., Jain, R.A., Marsden, K.C., Bell, H., Skinner, J., Hayer, K.E., Hogenesch, J.B., and Granato, M. (2015). A genome-wide screen identifies PAPP-AA-mediated IGFR signaling as a novel regulator of habituation learning. Neuron *85*, 1200–1211.
25. Burgess, H.A., and Granato, M. (2007). Modulation of locomotor activity in larval zebrafish during light adaptation. J. Exp. Biol. *210*, 2526–2539.
26. Jain, R.A., Wolman, M.A., Schmidt, L.A., Burgess, H.A., and Granato, M. (2011). Molecular-genetic mapping of zebrafish mutants with variable phenotypic penetrance. PLoS ONE *6*, e26510.
27. Tfelt-Hansen, J., and Brown, E.M. (2005). The calcium-sensing receptor in normal physiology and pathophysiology: a review. Crit. Rev. Clin. Lab. Sci. *42*, 35–70.
28. Herberger, A.L., and Loretz, C.A. (2013). Morpholino oligonucleotide knockdown of the extracellular calcium-sensing receptor impairs early skeletal development in zebrafish. Comp. Biochem. Physiol. A Mol. Integr. Physiol. *166*, 470–481.
29. Vizard, T.N., O'Keeffe, G.W., Gutierrez, H., Kos, C.H., Riccardi, D., and Davies, A.M. (2008). Regulation of axonal and dendritic growth by the extracellular calcium-sensing receptor. Nat. Neurosci. *11*, 285–291.
30. Yano, S., Brown, E.M., and Chattopadhyay, N. (2004). Calcium-sensing receptor in the brain. Cell Calcium *35*, 257–264.

31. Zhang, Z., Qiu, W., Quinn, S.J., Conigrave, A.D., Brown, E.M., and Bai, M. (2002). Three adjacent serines in the extracellular domains of the CaR are required for L-amino acid-mediated potentiation of receptor function. J. Biol. Chem. *277*, 33727–33735.
32. Phillips, C.G., Harnett, M.T., Chen, W., and Smith, S.M. (2008). Calcium-sensing receptor activation depresses synaptic transmission. J. Neurosci. *28*, 12062–12070.
33. Smith, S.M., Chen, W., Vyleta, N.P., Williams, C., Lee, C.-H., Phillips, C., and Andresen, M.C. (2012). Calcium regulation of spontaneous and asynchronous neurotransmitter release. Cell Calcium *52*, 226–233.
34. Eaton, R.C., DiDomenico, R., and Nissanov, J. (1991). Role of the Mauthner cell in sensorimotor integration by the brain stem escape network. Brain Behav. Evol. *37*, 272–285.
35. Kimmel, C.B., Hatta, K., and Metcalfe, W.K. (1990). Early axonal contacts during development of an identified dendrite in the brain of the zebrafish. Neuron *4*, 535–545.
36. Burgess, H.A., Johnson, S.L., and Granato, M. (2009). Unidirectional startle responses and disrupted left-right co-ordination of motor behaviors in *robo3* mutant zebrafish. Genes Brain Behav. *8*, 500–511.
37. Marsden, K.C., and Granato, M. (2015). In vivo Ca(2+) imaging reveals that decreased dendritic excitability drives startle habituation. Cell Rep. *13*, 1733–1740.
38. Kwong, R.W.M., Auprix, D., and Perry, S.F. (2014). Involvement of the calcium-sensing receptor in calcium homeostasis in larval zebrafish exposed to low environmental calcium. Am. J. Physiol. Regul. Integr. Comp. Physiol. *306*, R211–R221.
39. Jabeen, S., and Thirumalai, V. (2013). Distribution of the gap junction protein connexin 35 in the central nervous system of developing zebrafish larvae. Front. Neural Circuits *7*, 91.
40. Petrel, C., Kessler, A., Dauban, P., Dodd, R.H., Rognan, D., and Ruat, M. (2004). Positive and negative allosteric modulators of the Ca2+-sensing receptor interact within overlapping but not identical binding sites in the transmembrane domain. J. Biol. Chem. *279*, 18990–18997.
41. Kessler, A., Faure, H., Petrel, C., Ruat, M., Dauban, P., and Dodd, R.H. (2004). N2-benzyl-N1-(1-(1-naphthyl)ethyl)-3-phenylpropane-1,2-diamines and conformationally restrained indole analogues: development of calindol as a new calcimimetic acting at the calcium sensing receptor. Bioorg. Med. Chem. Lett. *14*, 3345–3349.
42. Conigrave, A.D., and Ward, D.T. (2013). Calcium-sensing receptor (CaSR): pharmacological properties and signaling pathways. Best Pract. Res. Clin. Endocrinol. Metab. *27*, 315–331.
43. Ray, K. (2015). Calcium-sensing receptor: trafficking, endocytosis, recycling, and importance of interacting proteins. Prog. Mol. Biol. Transl. Sci. *132*, 127–150.
44. Chen, C.J., Barnett, J.V., Congo, D.A., and Brown, E.M. (1989). Divalent cations suppress 3′,5′-adenosine monophosphate accumulation by stimulating a pertussis toxin-sensitive guanine nucleotide-binding protein in cultured bovine parathyroid cells. Endocrinology *124*, 233–239.
45. Mamillapalli, R., VanHouten, J., Zawalich, W., and Wysolmerski, J. (2008). Switching of G-protein usage by the calcium-sensing receptor reverses its effect on parathyroid hormone-related protein secretion in normal versus malignant breast cells. J. Biol. Chem. *283*, 24435–24447.
46. Ward, D.T. (2004). Calcium receptor-mediated intracellular signalling. Cell Calcium *35*, 217–228.
47. Rey, O., Young, S.H., Jacamo, R., Moyer, M.P., and Rozengurt, E. (2010). Extracellular calcium sensing receptor stimulation in human colonic epithelial cells induces intracellular calcium oscillations and proliferation inhibition. J. Cell. Physiol. *225*, 73–83.
48. Bai, M., Trivedi, S., Lane, C.R., Yang, Y., Quinn, S.J., and Brown, E.M. (1998). Protein kinase C phosphorylation of threonine at position 888 in Ca2+o-sensing receptor (CaR) inhibits coupling to Ca2+ store release. J. Biol. Chem. *273*, 21267–21275.
49. Pollak, M.R., Brown, E.M., Chou, Y.-H.W., Hebert, S.C., Marx, S.J., Steinmann, B., Levi, T., Seidman, C.E., and Seidman, J.G. (1993). Mutations in the human Ca(2+)-sensing receptor gene cause familial hypocalciuric hypercalcemia and neonatal severe hyperparathyroidism. Cell *75*, 1297–1303.
50. Nesbit, M.A., Hannan, F.M., Howles, S.A., Reed, A.A.C., Cranston, T., Thakker, C.E., Gregory, L., Rimmer, A.J., Rust, N., Graham, U., et al. (2013). Mutations in *AP2S1* cause familial hypocalciuric hypercalcemia type 3. Nat. Genet. *45*, 93–97.
51. Breitwieser, G.E. (2013). The calcium sensing receptor life cycle: trafficking, cell surface expression, and degradation. Best Pract. Res. Clin. Endocrinol. Metab. *27*, 303–313.
52. Wainwright, P.C., Ferry-Graham, L.A., Waltzek, T.B., Carroll, A.M., Hulsey, C.D., and Grubich, J.R. (2001). Evaluating the use of ram and suction during prey capture by cichlid fishes. J. Exp. Biol. *204*, 3039–3051.
53. Walker, J.A., Ghalambor, C.K., Griset, O.L., McKenney, D., and Reznick, D.N. (2005). Do faster starts increase the probability of evading predators? Funct. Ecol. *19*, 808–815.
54. Webb, P.W. (1984). Body and fin form and strike tactics of four teleost predators attacking fathead minnow (*Pimephales promelas*) prey. Can. J. Fish. Aquat. Sci. *41*, 157–165.
55. Herberholz, J., and Marquart, G.D. (2012). Decision making and behavioral choice during predator avoidance. Front. Neurosci. *6*, 125.
56. Mu, Y., Li, X.-Q., Zhang, B., and Du, J.-L. (2012). Visual input modulates audiomotor function via hypothalamic dopaminergic neurons through a cooperative mechanism. Neuron *75*, 688–699.
57. Rogers, R.D. (2011). The roles of dopamine and serotonin in decision making: evidence from pharmacological experiments in humans. Neuropsychopharmacology *36*, 114–132.
58. Mesce, K.A., and Pierce-Shimomura, J.T. (2010). Shared strategies for behavioral switching: understanding how locomotor patterns are turned on and off. Front. Behav. Neurosci. *4*, 49.
59. Sfar, S., Bzéouich, A.A., Kerkeni, E., Bouaziz, S., Najjar, M.F., Chouchane, L., and Monastiri, K. (2012). A novel *CASR* mutation in a Tunisian FHH/NSHPT family associated with a mental retardation. Mol. Biol. Rep. *39*, 2395–2400.
60. Conley, Y.P., Mukherjee, A., Kammerer, C., DeKosky, S.T., Kamboh, M.I., Finegold, D.N., and Ferrell, R.E. (2009). Evidence supporting a role for the calcium-sensing receptor in Alzheimer disease. Am. J. Med. Genet. B. Neuropsychiatr. Genet. *150B*, 703–709.
61. Kapoor, A., Satishchandra, P., Ratnapriya, R., Reddy, R., Kadandale, J., Shankar, S.K., and Anand, A. (2008). An idiopathic epilepsy syndrome linked to 3q13.3-q21 and missense mutations in the extracellular calcium sensing receptor gene. Ann. Neurol. *64*, 158–167.
62. Silve, C., Petrel, C., Leroy, C., Bruel, H., Mallet, E., Rognan, D., and Ruat, M. (2005). Delineating a Ca2+ binding pocket within the venus flytrap module of the human calcium-sensing receptor. J. Biol. Chem. *280*, 37917–37923.
63. Geng, Y., Mosyak, L., Kurinov, I., Zuo, H., Sturchler, E., Cheng, T.C., Subramanyam, P., Brown, A.P., Brennan, S.C., Mun, H.-C., et al. (2016). Structural mechanism of ligand activation in human calcium-sensing receptor. eLife *5*, e13662.
64. Zhang, C., Zhang, T., Zou, J., Miller, C.L., Gorkhali, R., Yang, J.-Y., Schilmiller, A., Wang, S., Huang, K., Brown, E.M., et al. (2016). Structural basis for regulation of human calcium-sensing receptor by magnesium ions and an unexpected tryptophan derivative co-agonist. Sci. Adv. *2*, e1600241.
65. Liu, X.-L., Lu, Y.-S., Gao, J.-Y., Marshall, C., Xiao, M., Miao, D.-S., Karaplis, A., Goltzman, D., and Ding, J. (2013). Calcium sensing receptor absence delays postnatal brain development via direct and indirect mechanisms. Mol. Neurobiol. *48*, 590–600.
66. Ruat, M., Molliver, M.E., Snowman, A.M., and Snyder, S.H. (1995). Calcium sensing receptor: molecular cloning in rat and localization to nerve terminals. Proc. Natl. Acad. Sci. USA *92*, 3161–3165.
67. Jones, B.L., and Smith, S.M. (2016). Calcium-sensing receptor: a key target for extracellular calcium signaling in neurons. Front. Physiol. *7*, 116.

68. Kavalali, E.T. (2015). The mechanisms and functions of spontaneous neurotransmitter release. Nat. Rev. Neurosci. *16*, 5–16.

69. Jin, I., Puthanveettil, S., Udo, H., Karl, K., Kandel, E.R., and Hawkins, R.D. (2012). Spontaneous transmitter release is critical for the induction of long-term and intermediate-term facilitation in *Aplysia*. Proc. Natl. Acad. Sci. USA *109*, 9131–9136.

70. Chang, W., Tu, C., Cheng, Z., Rodriguez, L., Chen, T.-H., Gassmann, M., Bettler, B., Margeta, M., Jan, L.Y., and Shoback, D. (2007). Complex formation with the type B gamma-aminobutyric acid receptor affects the expression and signal transduction of the extracellular calcium-sensing receptor. Studies with HEK-293 cells and neurons. J. Biol. Chem. *282*, 25030–25040.

71. Gama, L., Wilt, S.G., and Breitwieser, G.E. (2001). Heterodimerization of calcium sensing receptors with metabotropic glutamate receptors in neurons. J. Biol. Chem. *276*, 39053–39059.

72. Kohashi, T., and Oda, Y. (2008). Initiation of Mauthner- or non-Mauthner-mediated fast escape evoked by different modes of sensory input. J. Neurosci. *28*, 10641–10653.

73. Takahashi, M., Inoue, M., Tanimoto, M., Kohashi, T., and Oda, Y. (2017). Short-term desensitization of fast escape behavior associated with suppression of Mauthner cell activity in larval zebrafish. Neurosci. Res. *121*, 29–36.

74. Weiss, S.A., Preuss, T., and Faber, D.S. (2008). A role of electrical inhibition in sensorimotor integration. Proc. Natl. Acad. Sci. USA *105*, 18047–18052.

75. Koyama, M., Minale, F., Shum, J., Nishimura, N., Schaffer, C.B., and Fetcho, J.R. (2016). A circuit motif in the zebrafish hindbrain for a two alternative behavioral choice to turn left or right. eLife *5*, e16808.

76. von Reyn, C.R., Breads, P., Peek, M.Y., Zheng, G.Z., Williamson, W.R., Yee, A.L., Leonardo, A., and Card, G.M. (2014). A spike-timing mechanism for action selection. Nat. Neurosci. *17*, 962–970.

77. Neki, D., Nakayama, H., Fujii, T., Matsui-Furusho, H., and Oda, Y. (2014). Functional motifs composed of morphologically homologous neurons repeated in the hindbrain segments. J. Neurosci. *34*, 3291–3302.

78. Rauch, G.-J., Granato, M., and Haffter, P. (1997). A polymorphic zebrafish line for genetic mapping using SSLPs on high-percentage agarose gels. Tech. Tips Online *2*, 148–150.

79. Streisinger, G., Singer, F., Walker, C., Knauber, D., and Dower, N. (1986). Segregation analyses and gene-centromere distances in zebrafish. Genetics *112*, 311–319.

80. Pujol-Martí, J., Zecca, A., Baudoin, J.-P., Faucherre, A., Asakawa, K., Kawakami, K., and López-Schier, H. (2012). Neuronal birth order identifies a dimorphic sensorineural map. J. Neurosci. *32*, 2976–2987.

81. Hwang, W.Y., Fu, Y., Reyon, D., Maeder, M.L., Tsai, S.Q., Sander, J.D., Peterson, R.T., Yeh, J.-R.J., and Joung, J.K. (2013). Efficient genome editing in zebrafish using a CRISPR-Cas system. Nat. Biotechnol. *31*, 227–229.

82. Yamanaka, I., Miki, M., Asakawa, K., Kawakami, K., Oda, Y., and Hirata, H. (2013). Glycinergic transmission and postsynaptic activation of CaMKII are required for glycine receptor clustering in vivo. Genes Cells *18*, 211–224.

83. Neff, M.M., Turk, E., and Kalishman, M. (2002). Web-based primer design for single nucleotide polymorphism analysis. Trends Genet. *18*, 613–615.

84. Dosch, R., Wagner, D.S., Mintzer, K.A., Runke, G., Wiemelt, A.P., and Mullins, M.C. (2004). Maternal control of vertebrate development before the midblastula transition: mutants from the zebrafish I. Dev. Cell *6*, 771–780.

85. Mullins, M.C., Hammerschmidt, M., Haffter, P., and Nüsslein-Volhard, C. (1994). Large-scale mutagenesis in the zebrafish: in search of genes controlling development in a vertebrate. Curr. Biol. *4*, 189–202.

86. Lakhina, V., Marcaccio, C.L., Shao, X., Lush, M.E., Jain, R.A., Fujimoto, E., Bonkowsky, J.L., Granato, M., and Raper, J.A. (2012). Netrin/DCC signaling guides olfactory sensory axons to their correct location in the olfactory bulb. J. Neurosci. *32*, 4440–4456.

87. Labun, K., Montague, T.G., Gagnon, J.A., Thyme, S.B., and Valen, E. (2016). CHOPCHOP v2: a web tool for the next generation of CRISPR genome engineering. Nucleic Acids Res. *44* (W1), W272–W276.

88. Harris, J.A., Cheng, A.G., Cunningham, L.L., MacDonald, G., Raible, D.W., and Rubel, E.W. (2003). Neomycin-induced hair cell death and rapid regeneration in the lateral line of zebrafish (*Danio rerio*). J. Assoc. Res. Otolaryngol. *4*, 219–234.

89. Koyama, M., Kinkhabwala, A., Satou, C., Higashijima, S., and Fetcho, J. (2011). Mapping a sensory-motor network onto a structural and functional ground plan in the hindbrain. Proc. Natl. Acad. Sci. USA *108*, 1170–1175.

STAR★METHODS

KEY RESOURCES TABLE

REAGENT or RESOURCE	SOURCE	IDENTIFIER
Antibodies		
Rabbit anti-GFP	Life Technologies	A11122
Alexa488 Goat anti-Rabbit, highly cross-adsorbed	Life Technologies	A11034
Mouse anti-Cx35/36	Millipore	MAB3045
Alexa594 Goat anti-Mouse IgG, highly cross-adsorbed	Life Technologies	A11032
Anti-DIG-AP, Fab Fragment	Sigma	11093274910
Chemicals, Peptides, and Recombinant Proteins		
LOPAC-1280 small molecule library	Sigma	LO1280
Serotonin-HCl	Sigma	H9523
LY-165,163 (PAPP)	Sigma	S009
S15535	Sigma	S5321
R-(+)-7-Hydroxy-DPAT hydrobromide (7OHD)	Sigma	H168
U-99194A maleate	Santa Cruz Biotechnology	83598-46-3
Cas9 Protein	PNA Bio	CP02
BM Purple	Sigma	11442074001
Neomycin	Sigma	N1142
DASPEI	Invitrogen	D426
(+)-Tubocurarine Chloride	Millipore	505145
Calhex-231	Sigma	SML0668
NPS 2143 hydrochloride	Sigma	SML0362
Calindol hydrocholride	Santa Cruz Biotechnology	729610-18-8
Forskolin	Sigma	F6886
Rolipram	Sigma	R6520
U73122	Fisher	112648-68-7
phorbol 12-myristate 13-acetate (PMA)	Sigma	P8139
Experimental Models: Organisms/Strains		
Zebrafish: (Tüpfel Long Fin, TLF) wild type	[32]	ZFIN: ZDB-GENO-151014-6
Zebrafish: (WIK-L11) wild type	[78]	ZFIN: ZDB-GENO-010531-2
Zebrafish: *albino/slc45a2^{b4}; golden/slc24a5^{b1}; sparse/kita^{b5}*	[79]	ZFIN: ZDB-FISH-150901-5739; ZDB-FISH-150901-19447; ZDB-FISH-150901-23362
Zebrafish: *Tg(hsp70:GAL4FFDMC)130a; Tg(UAS:gap43-citrine)*	[80, 81]	ZFIN: ZDB-ALT-120320-6; ZDB-FISH-150901-21649
Zebrafish: *Tg(hsp70GFF62A); Tg(UAS:gcamp6s)*	[82, 47]	ZFIN: ZDB-ALT-150717-1; ZDB-TGCONSTRCT-160316-3
Zebrafish: *ignorance is bliss/ap2s1^{p172}*	[32]	ZFIN: ZDB-ALT-150701-2
Zebrafish: *wrong turn/CaSR^{p190}*	This paper	ZFIN: ZDB-ALT-171122-3
Zebrafish: *fashionably late^{p191}*	This paper	ZFIN: ZDB-ALT- 171122-4
Zebrafish: *procrastinator^{p192}*	This paper	ZFIN: ZDB-ALT- 171122-5
Zebrafish: *better late than never^{p193}*	This paper	ZFIN: ZDB-ALT- 171122-6
Zebrafish: *snooze button^{p194}*	This paper	ZFIN: ZDB-ALT- 171122-7
Zebrafish: *indecisive^{p195}*	This paper	ZFIN: ZDB-ALT- 180117-2
Zebrafish: *late responder^{p196}*	This paper	ZFIN: ZDB-ALT- 171122-8
Zebrafish: *biased^{dp197}*	This paper	ZFIN: ZDB-ALT- 180117-3
Zebrafish: *CaSR^{p198}*	This paper	ZFIN: ZDB-ALT- 180117-4

(*Continued on next page*)

Continued		
REAGENT or RESOURCE	SOURCE	IDENTIFIER
Zebrafish: *ap2s1*^{p199}	This paper	ZFIN: ZDB-ALT-180129-11
Oligonucleotides		
Primers for amplifying and genotyping *CaSR* & *ap2s1* mutations, see Table S3		
Recombinant DNA		
pDR274 plasmid	[81]	Addgene plasmid #42250
pDR274-CaSR sgRNA plasmid	This paper	N/A
pDR274-ap2s1 sgRNA plasmid	This paper	N/A
pCR2.1-CaSR	This paper	N/A
Software and Algorithms		
FLOTE & DAQTimer	[33]	https://science.nichd.nih.gov/confluence/display/burgess/Software
FasMotion	Fastec Imaging, Inc	http://www.highspeedimaging.com/fastec-software/
Imaris	Bitplane	http://www.bitplane.com/download
ChopChop v2	[41]	http://chopchop.cbu.uib.no/index.php
GraphPad Prism	GraphPad Software	https://www.graphpad.com/
dCAPS	[83]	http://helix.wustl.edu/dcaps/dcaps.html

CONTACT FOR REAGENT AND RESOURCE SHARING

Further information and requests for resources and reagents should be directed to and will be fulfilled by the Lead Contact, Michael Granato (granatom@pennmedicine.upenn.edu).

EXPERIMENTAL MODEL AND SUBJECT DETAILS

All experiments with zebrafish (*Danio rerio*) were approved by the University of Pennsylvania IACUC and/or the Haverford College IACUC. Wild-type Tüpfel Long-fin (TLF) and Wik-L11 (Wik) strains were used for all experiments [24, 78]. Embryos and larvae were raised at 29°C on a 14-h:10-h light:dark cycle in E3 media as previously described [24]. ENU mutagenesis was performed on TLF and Wik wild-type adult males using the protocol previously described [24, 84, 85]. The germline mutagenesis rate was measured by crossing mutagenized males to *albino*^{b4}; *golden*^{b1}; *sparse*^{b5} triple mutant females [84]. *Tg(hsp70:GAL4FFDMC)130a* and *Tg(hsp70:GFF62A)* were provided by Koichi Kawakami [80, 82]. *Tg(UAS:gap43-citrine)* fish were provided by Jonathan Raper [86]. *Tg(UAS:gcamp6s)* fish were previously described [37]. Sex is not determined in zebrafish until 25-60 dpf so behavioral analyses of larvae and juvenile fish were performed without consideration of sex.

To generate mutant alleles through CRISPR/Cas9 in this study, targeting sgRNA were designed using ChopChop v2 [87], cloned by direct annealing and ligation of oligos into pDR274 (Table S3) [81], synthesized using T7 MEGAshortscript kit (Ambion), and purified by MEGAclear kit (Ambion). Commercial Cas9 protein (PNA Bio) was combined with each sgRNA and injected into 1-cell stage wild-type TLF embryos (G0) to mutate the targeted genomic loci, and these mosaic G0 individuals were raised to adulthood and outcrossed to establish heterozygous carrier lines.

METHOD DETAILS

Behavioral recording

Larval and juvenile behavioral testing was performed as previously described [23, 24, 26], recorded from above at 1000fps or 500fps with either a Motionpro camera (Redlake) or a Fastec TS4 camera (Fastec Imaging). Larvae were held in individual 9 × 9mm wells of a laser-cut clear acrylic 4x4 testing arena mounted in a 6 cm Petri lid, resting on a metal ring attached to a vibration exciter (4810; Brüel and Kjaer, Norcross, GA) [26]. Constant infrared illumination below the testing arena was provided by a 96-bulb infrared LED array (IR100; YYtrade) with a white plexiglass sheet above it for even diffuse illumination, and a white light LED bulb (PAR38 LED light; LEDlight.com) obliquely lit the arena from above. Acoustic vibrational stimuli (2ms duration, 1000 Hz waveforms) were delivered vertically by the vibrational exciter. Visual "dark flash" stimuli were delivered by abruptly turning off the overhead white LED for 1 s, while the entire testing apparatus was shielded from ambient light by an opaque black vinyl enclosure. Acoustic and visual stimuli were controlled by a digital–analog card (PCI-6221; National Instruments, Austin, TX) using the DAQtimer program [25]. All acoustic stimuli were calibrated with a PCB Piezotronics accelerometer (#355B04) and signal conditioner (#482A21), and voltage outputs were converted to dB using the formula dB = 20 log(V/0.775). When measuring bias and responsiveness of larvae relative to varied stimulus intensities, the same larvae were exposed to all intensities of stimuli at 20 s interstimulus intervals to prevent habituation,

with intensities interleaved, 10 total stimuli per each intensity level. Temporal projections in Figure 1A were recorded at 1000 fps combining frames every 5 ms. Temporal projections in Figure 2B were recorded at 500 fps combining frames every 4 ms.

Genetic screen and mapping

ENU-mutagenized adult males from the TLF and WIK strains were crossed with wild-type females of the same strain, then inbred for three generations so that F3 offspring could be both screened for behavioral defects and used for molecular genetic mapping against F1 grandparents [24, 84, 85]. We screened 405 F2 families, with an estimated 614 mutagenized genomes screened. We measured the germline mutagenesis rate to be 0.09% by scoring crosses to *albino*^{b4}; *golden*^{b1}; *sparse*^{b5} triple mutants [84]. For each F3 clutch, we tested 32 larvae at 5 dpf for their acoustic response bias to 10 high intensity (25.9 dB) stimuli presented at 20 s ISI. We screened for clutches where at least 15%–25% of larvae showed a significantly divergent acoustic response bias from wild-type controls (typically individuals with acoustic startle biases < -40), indicating a recessive homozygous mutation affecting simple decision making. We validated F2 carriers by confirming similar frequencies of behaviorally mutant offspring in 2 or more independent crosses, and we collected behaviorally mutant and sibling F3 individuals from each family for genetic mapping and sequencing. Any larvae displaying striking morphological phenotypes, strong kinematic defects in the stereotyped performance of SLC or LLC behaviors, hearing defects, and/or low (< 40%) overall response rates to strong stimuli, were excluded from analysis. We further confirmed that each putative mutant was heritable by outcrossing the isolated F2 carriers of each family to wild-type TLF or WIK fish, then re-isolating new F3 adult carrier pairs that again produced clutches with the same decision-making defect in at least 15%–25% of their (F4) offspring. Whole genome sequencing was performed on gDNA from a pool of 50 behaviorally-selected *wrong turn* or *ignorance is bliss* F3 larvae, sequenced with 100 bp paired-end sequencing on the Illumina HiSeq 2000 platform, and homozygosity analysis done using 463,379 SNP markers identified by sequencing gDNA from ENU-mutagenized TLF and WIK males as described previously [24]. In parallel, independent gDNA pools of 50 behaviorally-selected mutant and sibling F3 larvae were screened by PCR for linkage to a panel of 147 SSLP markers across the zebrafish genome through bulk segregant analysis [24, 26]. Candidate mutations were defined as those SNPs from the whole genome sequencing that were linked to the identified SSLP markers with < 1% allele frequency in our reference sequence and > 95% allele frequency in the mutant sample that altered the amino acid sequence (nonsense, missense, or splice site mutations). Complementation between mutant lines was assessed by crossing verified heterozygous carriers between mutants and analyzing 1-4 crosses with 48-64 offspring each for behavioral bias to 10 high intensity (25.9 dB) stimuli presented at 20 s ISI. Alleles were classified as complementing if < 10% of each clutch showed a behavioral bias shift relative to wild-type controls.

Pharmacology

The LOPAC-1280 library (Sigma) was used for the small molecule screen as previously described [23]. Wild-type TLF fish in E3 embryo media were treated with 1:100 dilution of the stock concentration, typically producing a 10 μM final drug concentration in 1% DMSO. 8 wild-type fish were tested per compound in the screen. For chronic treatment of fish with *CaSR* antagonists, sets of 25 embryos were treated in 8ml E3 plus 80μl drug in DMSO starting at 24 hpf. Bath E3 was exchanged daily with fresh E3 + drug. Experiments using R-(+)-7-Hydroxy-DPAT hydrobromide (7OHD, Sigma), PAPP (LY-165,163, Sigma), S15535 (Sigma), U-99194A maleate (Santa Cruz), calindol hydrochloride (Sigma), forskolin (Sigma), rolipram (Sigma), U73122 (Fisher), and phorbol 12-myristate 13-acetate (PMA, Sigma) were performed by treating wild-type TLF larvae with indicated final concentrations of drug in E3 embryo media for 20 minutes prior to behavioral testing in the E3 medium still containing the drug (30 minutes for calindol). Experiments using Calhex-231 (Sigma) and NPS2143 hydrocholoride (Sigma) were performed by treating embryos and/or larvae for the noted time periods. When treatment lasted longer than 1 day, fresh drug and E3 (or DMSO & E3 for controls) was replaced each day, and for 24-112 hpf treatments E3 containing drug was removed at 112 hpf and rinsed 3 times with fresh E3 + DMSO. For all drug experiments, the final DMSO concentration in E3 was 1% for drug-treated and control fish. For lateral line ablation, 40 μM neomycin (Sigma, N1142) was applied to 6 dpf larvae in E3 for 1 hour at 29°C. Larvae were washed 4x with E3 and given 3-4 hours recovery time at 29°C before behavioral testing. After testing, DASPEI (Invitrogen, D 426) staining of neuromasts was performed to confirm complete ablation, incubating larvae in 0.05% DASPEI in E3 for 15 min, followed by 2 E3 washes prior to imaging [88].

Mutant Genotyping

CaSR^{p190} fish were genotyped either using the KASP method with proprietary primer sequences (LGC Genomics), or by amplifying the genomic locus with primers designed through the dCAPS program [83] followed by digestion by HinfI (NEB) to specifically digest the mutant allele (Table S3). The *ap2s1*^{p172} allele was genotyped by amplifying with dCAPS-designed primers (Table S3) followed by digestion by BsmAI (NEB) to specifically digest the mutant allele. CRISPR-generated mutant alleles were identified by amplifying the targeted region (see Table S3) and testing for a loss of a restriction site (BsaJI for *CaSR*^{p198}, MscI for *ap2s1*^{p199}).

Immunofluorescent Imaging

Larvae were fixed for 4 hours at room temperature in Sweet Fix (4% paraformaldehyde, 4% sucrose, 1x PBS pH 7.4) then brains were manually exposed by peeling away skin and jaw parts surrounding the brain with fine forceps. Tissue was permeabilized for 45 minutes with 0.1% collagenase in PBS (Sigma C-9891), then blocked in incubation buffer (0.2% BSA, 2% normal goat serum, 0.5% Triton X-100, 1% DMSO in 1x PBS pH 7.4). Antibodies were diluted in incubation buffer and then used to detect their antigens in the fixed, dissected brains using Rabbit anti-GFP (1:500, Life Technologies) and Mouse anti-Cx35/36 (1:200, Millipore) primary

antibodies, and Alexa488 Goat anti-Rabbit and Alexa594 Goat anti-Mouse IgG, highly cross-adsorbed secondary antibodies (1:500, Life Technologies). Brains were then mounted in vectashield (Vector Labs), saving the individual tails matching each brain for subsequent genotyping. Images were acquired using a Zeiss LSM-710 confocal microscope.

In situ hybridization

To generate a probe for *CaSR* mRNA, we first amplified wild-type zebrafish *CaSR* cDNA containing the full coding sequence and a portion of the 3′UTR from 120 hpf larval total RNA using *CaSR* cDNA cloning primers (Table S3) and directly cloned it into pCRII-TOPO (ThermoFisher). We linearized the plasmid with BamHI (NEB), and synthesized an antisense DIG-labeled RNA probe using T7 RNA polymerase (Promega). Larvae were raised in E3 with 0.003% phenylthiourea to minimize pigment development, then were fixed in 4% paraformaldehyde/PBS and stored in methanol at −20°C. Larvae were permeabilized with 0.1% collagenase in 1x PBS for 2 hours, washed with PBS+0.1% Tween-20, then prehybridized at 65°C in hybridization solution [50% formamide, 5 × SSC buffer, 50 μg/ml heparin, 5 mg/ml torula yeast RNA, 0.1% Tween-20, pH 6.0 adjusted with citric acid], followed by overnight incubation in hybridization buffer with DIG-labeled probe RNA at 65°C. Larvae were washed at 65°C with 50% formamide/2 × SSC/0.1% Tween-20, then 2 × SSC/0.1% Tween-20, then 0.2 × SSC/0.1% Tween-20, followed by room temperature washing in MABT [100 mM maleic acid, 150 mM NaCl, 0.1% Tween-20, pH 7.5], blocking in MABT supplemented with 2% BM Block reagent (Sigma), 5% Normal Goat Serum, 2 mg/ml BSA, then overnight incubation with anti-DIG-AP antibody (1:3000, Roche) in blocking solution at room temperature. Larvae were washed with MABT then TMNT [100 mM Tris pH 9.5, 50 mM $MgCl_2$, 100 mM NaCl, 0.1% Tween-20, 1mM levamisole], and probe was detected with BM Purple reagent (Sigma). Stained larvae were mounted in 70% glycerol and imaged with a SPOT Insight 2Mp camera.

Calcium Imaging

Mauthner calcium imaging and analysis was performed as previously detailed [37]. Larvae were semi-restrained in 2% low melting point agarose with tails freed distal to the swim bladder. GCaMP6s images were captured with a Leica DM16000 B inverted spinning disk confocal at 20 Hz and tail movements with a Dalsa Genie HM640 camera at 500 Hz. We stimulated head-restrained larvae with 13.1 dB (intense) or −15 dB (subthreshold) acoustic stimuli, separating stimuli by at least 3 minutes to avoid habituation.

Electrophysiology

Electrophysiological recordings were conducted on wild-type and $CaSR^{p190}$ mutant 5–6 dpf zebrafish, blind to *CaSR* genotype. Each larva also expressed membrane-targeted citrine in the Mauthner neurons for visualization: *Tg(hsp70:GAL4FFDMC)130a; Tg(UAS:gap43-citrine)*. Larvae were paralyzed with d-tubocurarine (10 μM, Sigma) in external solution (in mM: 134 NaCl, 2.9 KCl, 2.1 $CaCl_2$, 1.2 $MgCl_2$, 10 HEPES, 10 Glucose, pH 7.8 adjusted with NaOH) then placed on their backs and held with pins in a Sylgard-coated small culture dish (FluoroDish, WPI). The brain was exposed ventrally following the procedure described by Koyama et al. [89]. Next, the dish containing the larvae was placed in the recording setup and superfused with external solution throughout the recording session. The Mauthner were identified by far-red DIC optics and citrine fluorescence. The patch pipette (3-4 MΩ) was filled with internal solution (in mM: 105 K-Methanesulfonate, 10 HEPES, 0.1 EGTA, 2 $MgCl_2$, 4 Na_2ATP, 0.4 Tris-GTP, 10 K_2-Phosphocreatine, 23 mannitol, pH 7.2 adjusted with KOH). The liquid junction potential was estimated in −16 mV using Clampex 10.6 (Molecular Devices). Whole-cell recordings were performed under current-clamp configuration and the bridge balance adjusted. The rheobase, defined as the minimum amount of positive current required to elicit an action potential, was determined by delivering a 10 ms current pulse of increasing magnitude. The voltage threshold was defined as the membrane potential value at which the depolarizing-current step elicits an action potential. The input resistance was estimated using the voltage deflection caused by a hyperpolarizing-current step of −1 nA and 10 ms duration, followed by derivation of resistance with Ohm's law. Recordings were performed on a single Mauthner neuron per larva, and larval genotypes were determined for each individual tested after analysis was complete.

QUANTIFICATION AND STATISTICAL ANALYSIS

Statistical analysis was performed using Graphpad Prism 6 and Microsoft Excel 14.1. Box-and-whisker plots indicate the median with whiskers extending to minimum and maximum data points. Error bars on bar plots and dot plots always indicate SEM. Student's two-tailed t test with Welch's correction for unequal variance was used in pairwise comparisons unless otherwise stated, using the Bonferroni correction for multiple comparisons where appropriate. Fisher's Exact Test was used to look for over-representation of drug targets from the LOPAC-1280 library and pectoral fin usage with Prism. The Kruskal Wallis test was used to examine the impact of varying stimulus intensity on larval startle bias using Prism. Statistical significance was defined as $p < 0.05$ in each statistical test, and the significance is shown within figures and/or in the figure legends.

Behavioral Analyses

5-7 dpf larval behavior was tracked and scored using Flote software [25], while juvenile fish behavior and all pectoral fin movement scoring was performed manually, blind to genotype. To test startle bias, fish were exposed to 10 identical acoustic stimuli at 20 s Inter-Stimulus Intervals (ISI). Relative Startle Bias Index was calculated using the formula: 100% × (SLC frequency – LLC frequency)/(total SLC + LLC response frequency), producing a range from +100% (all SLC) to −100% (all LLC). To test acoustic habituation of decision-making mutants with a baseline inherent bias toward LLC behavior that performed few SLC responses, we

calculated the habituation of the *total* acoustic response rate (SLC and LLC behaviors combined) using the formula: 100% × (% Total responses to stimuli 31-40 at 1-s ISI)/(% Total baseline responses to stimuli 1-10 at 20-s ISI). Unless otherwise specified, mutant data presented consists of individuals that were tested and scored blindly then molecularly genotyped (where mutations were known) after all testing was complete. For secondary behavioral characterization presented in Table 1, larvae were generated from adult carriers 1-4 generations subsequent to the F2 generation of the initial screen shown in Figure 2A. Relative Bias and Total Response % in Table 1 were calculated from the larvae with the lowest 25% Relative Bias in the clutch of carriers. The remaining behaviors of Table 1 were tested on behaviorally-selected individuals with Relative Bias (26 dB) of +100% for siblings and < −60% for mutants. Since *biased*^{dp197} showed a clear dominant phenotype in heterozygotes, larval progeny of *biased*^{dp197} heterozygous carriers crossed to wild-type are presented in Table 1. All *CaSR* mutant data presented in Table 1 were from subsequently genotype-verified larvae. Spontaneous activity was calculated by measuring average distance traveled per second over 160 s.

LOPAC-1280 Chemical Screen

Larvae responding to < 50% of strong stimuli (20-s ISI) were excluded from analysis, and compounds where treatment resulted in < 3 analyzable individuals were also excluded. For each treatment, 3 Z-scores of the bias change relative to all other tested and analyzed sibling fish tested that day were calculated using the following formula: Z-score = (Treated Bias – Avg Bias of Experimental Day)/(Std Deviation of Bias for Experimental Day), with typically 450-600 analyzable fish per experimental day. Z_{weak} examined responses to 10 weak stimuli (5-10 dB at 20-s ISI), Z_{strong} examined responses to 10 strong stimuli (25.9 dB at 20-s ISI), and $Z_{habituation}$ was the average Z-score across 3 blocks of 10 habituating strong stimuli (25.9 dB, 1-s ISI, 30 total stimuli).

Mauthner Structural Imaging

Confocal stacks were used to quantify Mauthner morphology with Imaris 8 software (Bitplane) by creating a Mauthner surface based on the anti-GFP immunofluorescent signal from *Tg(GFFDMC130A);Tg(UAS:gap43-citrine)* expression. The lateral dendrite (LD) was manually segmented from the Mauthner with a vertical plane at 30μm from the most lateral distal point along the axis of the Mauthner soma, which included all club ending synapses into the LD region in all samples. The ventral dendrite (VD) was manually segmented by creating a cut plane at the inflection point between the ventral dendrite and the soma. The remaining central portion was defined as the soma. Neighboring blood cells occasionally labeled in this transgenic line were manually masked as necessary to avoid distorting quantifications. Quantification of Cx35 was performed through Imaris by first using the Mauthner surface to mask the Cx35 signal to isolate signal within the Mauthner neuron, then measuring total Cx35 signal in each segmented region. We manually measured Cx35-labeled club endings by creating surfaces from the masked Cx35 channel and counting the number of surfaces on the LD that had volumes greater than 750 voxels. Segmenting, masking, and quantification were performed blind to genotype.

Calcium Imaging

Behavioral latency was determined by manually examining tail videos for the first frame of tail movement, and GCaMP6s fluorescence changes were analyzed using ImageJ (NIH). Identically sized ROIs were manually created for the Mauthner soma and background, and the mean pixel value of the background ROI was subtracted from the mean of each target ROI for all images in the sequence to calculate the intensity at each time point. F_0 was calculated by averaging the intensity of the 20 time points (1 s) immediately prior to the acoustic stimulus. We defined Mauthner firing as a fluorescence change $\Delta F/F > 0.4$ in the soma, above which 95% of contralateral short-latency (< 10 ms) responses fell for siblings and no instances of long-latency responses or non-responses exceeded this. Imaging and analysis was performed blind to genotype, and each larva was genotyped after completion of the analyses.